

1 **High time-resolved measurement of stable carbon isotope**
2 **composition in water-soluble organic aerosols: method optimization**
3 **and a case study during winter haze in East China**

4 Wenqi Zhang^{1,2,3}, Yan-Lin Zhang^{1,2,3*}, Fang Cao^{1,2,3}, Yankun Xiang^{1,2,3}, Yuanyuan
5 Zhang^{1,2,3}, Mengying Bao^{1,2,3}, Xiaoyan Liu^{1,2,3}, Yu-Chi Lin^{1,2,3}

6 1Yale–NUIST Center on Atmospheric Environment, International Joint Laboratory on Climate and
7 Environment Change (ILCEC), Nanjing University of Information Science and Technology,
8 Nanjing 210044, China

9 2Key Laboratory of Meteorological Disaster, Ministry of Education (KLME)/ Collaborative
10 Innovation Center on Forecast and Evaluation of Meteorological Disasters (CIC-FEMD), Nanjing
11 University of Information Science and Technology, Nanjing 210044, China

12 3Jiangsu Provincial Key Laboratory of Agricultural Meteorology, College of Applied Meteorology,
13 Nanjing University of Information Science and Technology, Nanjing 210044, China

14
15 **Abstract:** Water soluble organic carbon (WSOC) is a significant fraction of organic carbon (OC) in
16 atmospheric aerosols. WSOC is of great interest due to its significant effects on atmospheric
17 chemistry, the Earth's climate and human health. Stable carbon isotope ($\delta^{13}\text{C}$) can be used to track
18 the potential sources and investigate atmospheric processes of organic aerosols. However, the
19 previous methods measuring the $\delta^{13}\text{C}$ values of WSOC in ambient aerosols require large amount of
20 carbon contents as well as time-consuming and labor-intensive preprocessing. In this study, a
21 method of simultaneously measuring the mass concentration and the $\delta^{13}\text{C}$ values of WSOC from
22 aerosol samples is established by coupling the Gas Bench II preparation device with isotopic ratio
23 mass spectrometry. The precision and accuracy of isotope determination is better than 0.17 ‰ and
24 0.5 ‰, respectively, for samples containing WSOC larger than 5 μg . This method is then applied
25 for the aerosol samples collected every 3 hours during a severe wintertime haze period in Nanjing,
26 East China. WSOC varies between 3-32 $\mu\text{g m}^{-3}$, whereas $\delta^{13}\text{C}_{\text{-WSOC}}$ ranges from -26.24 ‰ to -
27 23.35 ‰. Three different episodes (e.g., namely the Episode 1, the Episode 2, the Episode 3) are
28 identified in the sampling period, showing a different tendency of $\delta^{13}\text{C}_{\text{-WSOC}}$ with the accumulation
29 process of WSOC aerosols. The increases in both the WSOC mass concentrations and the $\delta^{13}\text{C}_{\text{-WSOC}}$

30 values in the Episode 1 indicate that WSOC is subject to a substantial photochemical aging during
31 the air mass transport. In the Episode 2, the decline of the $\delta^{13}\text{C}_{\text{WSOC}}$ is accompanied by the increase
32 in the WSOC mass concentrations, which is associated with regional-transported biomass burning
33 emissions. In the Episode 3, heavier isotope (^{13}C) is exclusively enriched in total carbon (TC)
34 compares to WSOC aerosols. This suggests that non-WSOC fraction in total carbon may contain
35 ^{13}C -enriched components such as dust carbonate which is supported by the enhanced Ca^{2+}
36 concentrations and air mass trajectories analysis. The present study provides a novel method to
37 determine the stable carbon isotope composition of WSOC and it offers a great potential to better
38 understand the source emission, the atmospheric aging and the secondary production of water
39 soluble organic aerosols.

40 **Key words:** WSOC, stable carbon, $\delta^{13}\text{C}$, aging

41

42 **1. Introduction**

43 Water soluble organic carbon (WSOC) contributes a large fraction (9-75 %) to the organic
44 carbon (OC) (Anderson, et al., 2008; Decesari et al., 2007; Sullivan et al., 2004) and affects
45 substantially the global climate change and human health (Myhre, 2009; Ramanathan et al., 2001).
46 Due to its hydrophilic nature, WSOC has a great impact on the hygroscopic properties of aerosols
47 and promotes to increase the cloud condensation nuclei (CCN) activity (Asa-Awuku et al., 2011).
48 WSOC is a contributor to cardiovascular and respiratory problems because it is easy to be
49 incorporated in biological systems such as human blood and lungs (Mills et al., 2009).

50 WSOC can be emitted as primary organic carbon (POC) and secondary organic carbon (SOC)
51 produced from atmospheric oxidation of volatile organic compounds (VOCs) (Sannigrahi et al.,
52 2006; Weber et al., 2007; Zhang et al., 2018). Due to the hygroscopic property of the WSOC, the
53 origins of POC may be from biomass burning or marine emissions. However, the SOC may stem
54 from various sources including coal combustion, vehicle emissions, biogenic emissions, marine
55 emissions and biomass burning (Kirillova et al., 2010, 2013; Jimenez et al., 2009; Decesari et al.,
56 2007; Bozzetti et al., 2017b; Bozzetti et al., 2017a).

57 Stable carbon isotopic composition ($\delta^{13}\text{C}$) can provide valuable information to track both
58 potential sources and atmospheric processes of carbonaceous aerosols (Rudolph, 2007; Pavuluri and
59 Kawamura, 2012; Kirillova et al., 2013; Kirillova et al., 2014). Carbonaceous aerosols from coal
60 combustion have an isotope signature from -24.9 ‰ to -21 ‰ (Cao et al., 2011). Particulate matter
61 emitted from motor vehicles exhibits with isotopes from -26 ‰ to -28 ‰ (Widory, 2006),
62 respectively. Due to the different pathways of metabolism, C3 and C4 plants exhibit significant
63 differences of $\delta^{13}\text{C}$ (approximately -27 ‰ for C3 and -13 ‰ for C4, [Martinelli et al., 2002; Sousa
64 Moura et al., 2008]). Laboratory studies demonstrate that there is no significant isotope fractionation
65 (± 0.5 ‰) between the produced aerosols and the C3 plants material (Turekian et al., 1998; Currie
66 et al., 1999; Das et al., 2010). While the C4 plants burning results in ^{13}C depletion (< 0.5 to 7.2%)
67 in the produced aerosols (Turekian et al., 1998; Das et al., 2010). Marine organic aerosol sources
68 have a carbon isotope signature of -22 ‰ to -18 ‰, (Miyazaki et al., 2011) and play an important
69 role in the aerosols at coastal sites. In contrast, carbonate carbon exhibits with pretty high isotopic
70 ratio of -0.3 ‰ (Kawamura et al., 2004), and generally shows a large proportion in dust aerosols.
71 Thus, the isotope signatures of particulate matter emitted from these various sources may have
72 different effect on the characteristics of $\delta^{13}\text{C}$ in ambient WSOC.

73 In addition, atmospheric processes like secondary formation and photochemical aging may
74 change the constitution and properties of WSOC, as well as the stable carbon isotope of WSOC
75 ($\delta^{13}\text{C}_{\text{WSOC}}$). According to the kinetic isotope effect (KIE), the reaction rate of molecules containing
76 heavier isotopes is usually lower than the molecules containing lighter isotopes (Atkinson R., 1986;
77 Kirillova et al., 2013; Fisseha et al., 2009). The change in reaction rate is primarily results from the
78 greater energetic need for molecules containing heavier isotopes to reach the transition state (Nina
79 et al., 1979). Consequently, the oxidants preferentially react with molecules with lighter isotopes
80 (inverse kinetic isotope effect, KIE), which would result in an enrichment of ^{13}C in the residual
81 materials and a depletion in ^{13}C of the particulate oxidation products (Rudolph et al., 2002).
82 Therefore, organic compounds formed via secondary formation are generally depleted in ^{13}C
83 compared with their precursors (Sakugawa and Kaplan, 1995, Fisseha et al., 2009) and this isotope
84 depletion has proven by both field measurements and laboratory studies (Pavuluri and Kawamura,
85 2012). For example, the studies of KIE clearly indicate that the compounds formed via the oxidation

86 are depleted in the ^{13}C compared with their precursors during the reaction of VOCs with OH and
87 ozone (dominant atmospheric oxidants) (Iannone et al., 2003; Rudolph et al., 2000; Anderson et al.,
88 2004; Fisseha et al., 2009). Whereas an enrichment of ^{13}C in the particulate organic aerosol may
89 occur in the atmospheric aging processes, such as interactions with photochemical oxidants (e.g.
90 hydroxyl radical and ozone) during the long range transport. For instance, studies have demonstrated
91 that the substantial enrichment of ^{13}C in the residual, aged aerosols (e.g. isoprene, a precursor of
92 oxalic acid (Rudolph et al., 2003) after a long range transport. In that case, the stable carbon isotope
93 can be used to study the sources and the atmospheric processes that contribute to the carbonaceous
94 aerosols.

95 Several studies report the temporal and spatial variation, complex chemical species, light
96 absorption and thermal characteristics of WSOC, as well as its relationship with other compounds
97 in fine particles (Wozniak et al., 2008; Wang et al., 2006; Zhang et al., 2018; Martinez et al., 2016).
98 However, only few studies focus on the analysis of $\delta^{13}\text{C}_{\text{WSOC}}$ (Fisseha et al., 2006; Kirillova et al.,
99 2010; Suto et al., 2018; Lang et al., 2012; Zhou et al., 2015). This is partially due to the limited
100 techniques to analyze the $\delta^{13}\text{C}$ signatures of WSOC in ambient aerosols, as their concentrations are
101 usually very small. In the recent years, some efforts have been made to measure the $\delta^{13}\text{C}$ values of
102 WSOC. Bauer et al. (1991) uses potassium persulfate to convert organic carbon in natural waters
103 into CO_2 for $\delta^{13}\text{C}$ measurements. This wet oxidation method requires more than 0.5mM C and 1h
104 during the pretreatment (from sample injection to the isolation of purified CO_2). Fisseha et al. (2006)
105 boiled the oxidizing solution for 45 min to remove the organic matter and the total time required for
106 the pretreatment (for 15 samples) is 1.5h. Kirillova et al (2010) develops a combustion method that
107 applies the aerosol extract without filtration for isotope measurement and involves complicated
108 processes such as the freeze-drying of the aerosol extract under vacuum for 16 h. This combustion
109 method is the most widely used for the $\delta^{13}\text{C}$ measurements in WSOC aerosols (Kirillova et al., 2010,
110 2013, 2014; Miyazaki et al., 2012; Pavuluri et al., 2017). Although these methods are able to provide
111 the $\delta^{13}\text{C}$ values of WSOC in natural waters and/or ambient aerosols, the analytical methods require
112 either large amount of WSOC (from 100 $\mu\text{g C}$ to 0.5 mM C) or time-consuming preprocessing. And
113 some of the methods oxidize the WSOC extract without filtration and/or decarbonation in the
114 pretreatment., which would result in higher uncertainty of the $\delta^{13}\text{C}$ results. The high detection limit

115 of the previous methods is difficult to determine the $\delta^{13}\text{C}_{\text{WSOC}}$ in aerosol samples with low carbon
116 concentrations. In that case, an easily operated method detecting the $\delta^{13}\text{C}_{\text{WSOC}}$ values in aerosol
117 samples with low detection limit and high precision is urgently needed. The objectives of this study
118 are: 1) to provide an accurate, precise and easily operated method to measure the WSOC and $\delta^{13}\text{C}_{\text{WSOC}}$
119 in ambient aerosol samples. 2) to apply this method for analyzing the high time resolution
120 aerosol samples during a severe haze and discuss the potential sources and the atmospheric
121 processes of WSOC. In addition, the concentrations of inorganic ions and air mass back trajectories
122 coupled with MODIS fire maps are also analyzed to substantiate the results obtained from the $\delta^{13}\text{C}$
123 analysis.

124 **2. Methods**

125 2.1 Standards

126 Four working standards are used in this study: potassium hydrogen phthalate (KHP), benzoic
127 acid (BA), sucrose ($\text{C}_6\text{H}_{12}\text{O}_6$) and sodium oxalate (C_2). KHP and BA are widely used as the standards
128 of WSOC measurements (Kirillova et al., 2010) and then are used here as the WSOC test substances.
129 Also, their isotope signatures are close to the $\delta^{13}\text{C}$ values of aerosol samples (Miyazaki et al., 2012;
130 Fisseha et al., 2009; Suto et al., 2018). Sucrose and oxalic are taken as the standards to represent the
131 characteristics of the components in atmospheric WSOC (Fowler et al., 2018; Liang et al., 2015;
132 Pathak et al., 2011; Pavuluri and Kawamura, 2012). The carbon isotope composition of these four
133 standards are: -12.20 ‰ ($\text{C}_6\text{H}_{12}\text{O}_6$), -13.84 ‰ (C_2), -27.17 ‰ (BA) and -30.40 ‰ (KHP), respectively.
134 The wide range of the delta values of the working standards is able to cover the majority of the $\delta^{13}\text{C}_{\text{WSOC}}$
135 values in ambient aerosol samples. Standards are resolved in Milli-Q water (18.2 M Ω quality)
136 to make standard solutions of 0.25 $\mu\text{g mL}^{-1}$, 0.75 $\mu\text{g mL}^{-1}$, 1.5 $\mu\text{g mL}^{-1}$, 3 $\mu\text{g mL}^{-1}$, 6 $\mu\text{g mL}^{-1}$, 12 μg
137 mL^{-1} and 24 $\mu\text{g mL}^{-1}$, which means containing carbon content of 1 μg , 3 μg , 6 μg , 12 μg , 24 μg , 48 μg
138 and 96 μg in 4 mL standard solution to test the procedures during the pretreatment.

139 2.2 Aerosol samples

140 The aerosol samples are collected during a severe haze in January (from Jan 14th to 28th) of
141 2015 at the suburban of Nanjing, a megacity in East China. The sampling site is located at the
142 Agrometeorological station in the campus of the Nanjing University of Information Science and
143 Technology. It is close to a busy traffic road and surrounded by a large number of industrial factories.
144 $\text{PM}_{2.5}$ samples are collected on pre-combusted quartz-fiber filters (180 \times 230 mm) every 3 hours with

145 a high-volume aerosol sampler (KC100, Qingdao, China) at a flow rate of $1 \text{ m}^3 \text{ min}^{-1}$. After
146 sampling, all the filters are wrapped in the aluminum foil, sealed in air-tight polyethylene bags and
147 stored at $-26 \text{ }^\circ\text{C}$ for later analysis. A field blank is obtained by placing the blank filter in the filter
148 holder for 10 minutes without sampling.

149 2.3 Chemical analysis

150 $\text{PM}_{2.5}$ concentrations are observed at Pukoku Environmental Supervising Station.
151 Concentrations of total carbon (TC) and $\delta^{13}\text{C}_{\text{TC}}$ values are analyzed with EA-IRMS (Thermo Fisher
152 Scientific, Bremen, Germany). WSOC mass concentrations are measured with the TOC analyzer
153 (Shimadzu). Ion concentrations are obtained from Ion Chromatograph (IC, Thermo Fisher Scientific,
154 Bremen, Germany). Besides, the meteorological data are observed nearby the sampling site (Enivs
155 automatic meteorological station).

156 2.4 Sample pretreatment

157 The wet oxidation method is used to covert the WSOC to CO_2 (Sharp J. H., 1973), and the
158 resulting CO_2 can be measured by IRMS. The overview of the optimized method for measuring
159 WSOC and $\delta^{13}\text{C}_{\text{WSOC}}$ in the aerosols is shown in Fig. 1. The process of the pretreatment consists of
160 6 steps: WSOC on a 20 mm diameter disc is extracted with 6 mL mili-Q water through water-bath
161 ultrasonic for 30 minutes (step 1-2). The WSOC extract is filtered with a $0.22 \mu\text{m}$ syringe filter to
162 remove the particles in step 3. 2.0 g potassium persulfate ($\text{K}_2\text{S}_2\text{O}_8$, Aladdin Industrial Corporation,
163 Shanghai) and 100 μL phosphoric acid (85 % H_3PO_4 , AR, ANPEL Laboratory Technologies Inc.,
164 Shanghai) are dissolved in 50 mL Milli-Q water to make the oxidizing solution. The oxidizing
165 solution made within 24 h is added into the filtered WSOC extract as shown in step 4 of Fig. 1. The
166 phosphoric acid is added to remove the inorganic carbon resolved in the solution, and the persulfate
167 is added for the preparation to convert the organic compounds to CO_2 . The vials are sealed tightly
168 with the caps as soon as the oxidizing solution is added into the WSOC extract.

169 To remove the ambient CO_2 dissolved in the mixture (mixed solution of the oxidizing solution
170 and the WSOC extract) and the atmospheric CO_2 in the headspace of the sealed sample vials, high-
171 purity helium (Grade 5.0, 99.999 % purity) is flushed into the vials for 5 min in step 5. The aim of
172 this step is to exclude the possible contamination from the atmospheric CO_2 , and it has to be finished
173 within 12 hours after the mixture of the WSOC extract and the oxidizing solution to avoid the loss
174 of CO_2 produced under room temperature. High-purity helium ($15\text{-}18 \text{ mL min}^{-1}$) is flushed under

175 the water surface and a stainless steel tube is set for the output gas stream. The open end of this tube
176 is submerged in Milli-Q water to prevent any backflow of atmospheric CO₂ (Fig. 1., step 5). After
177 flushing, the vials are heated at 100 °C for 60 min in the sand bath pot (quartz sand, Y-2, Guoyu,
178 China) to start the oxidation of WSOC in step 6. The heated vials are stored overnight at room
179 temperature for condensing the moisture before the analysis on IRMS to prevent the damage to the
180 measuring equipment.

181 2.5 Determination of the carbon content and stable carbon isotopic ratios

182 CO₂ gas produced in the headspace of the prepared sample is extracted and purified by Gas
183 Bench II (Gas Bench II, Thermo Fisher Scientific, Bremen, Germany), and introduced into an
184 isotope ratio mass spectrometer (IRMS) (Mat 253, Thermo Fisher Scientific, Bremen, Germany)
185 for δ¹³C-CO₂ analysis. The extracted gas is purified with a Nafion water trap to remove the water
186 vapor and then the gas is loaded into a 100 uL sample loop through an eight-port Valco valve. After
187 120 s loading time (the duration time from the beginning of the analysis to the first rotation of the
188 eight port in the Gas Bench II.), the eight-port Valco valve rotates every 70 s to inject the sample
189 gas from the loop into a GC column (Poraplot Q fused-silica cap, 25 m, 0.32 mm; Agilent
190 Technologies). The GC column is set at 40 °C for the CO₂ separation from the matrix gases. The
191 separated CO₂ is introduced into another Nafion water trap and subsequently enters into the IRMS
192 with an open split. The CO₂ gas in each vial is detected 10 times in 15 minutes, showing 10 sample
193 peaks after five reference peaks. The peak areas and the isotope compositions of the 10 sample
194 peaks are given correspondingly, the results of the first two sample peaks are abandoned considering
195 the possible memory effect of the system. The average peak area and the isotope composition of the
196 last eight peaks is taken as the result of a certain sample determined by GB-IRMS.

197 **3. Method optimization**

198 The wet oxidation method is adapted from the stable isotope analysis of organic matter in
199 ground water (Lang et al., 2012; Zhou et al., 2015). Several tests are performed to adjust the optimal
200 conditions for measuring WSOC aerosols with relative low carbon amounts.

201 3.1 The carbon content in the procedural blank

202 In order to quantify the low concentration of WSOC in aerosols, it is critical to reduce the
203 carbon content in the procedural blank for minimizing the detection limit of the method. To achieve
204 this goal, the procedural blanks are analyzed to test the contamination that the reagents would

205 introduce to the results (shown in Table 1). The average carbon content in the procedural blank is
206 about 0.5 $\mu\text{g C}$ (corresponding with a peak area of 0.23 Vs) with a $\delta^{13}\text{C}$ value of $-27.04 \pm 1.28 \%$
207 ($n=15$). The carbon contents and the isotope compositions of Mili-Q water and the agents dissolved
208 in the oxidizing solution are also determined to identify the source of contamination in the
209 procedural blank. The peak area of Mili-Q water is not detected (Table. 1.) after going through all
210 the processes in the pretreatment without adding any other materials, suggesting no contamination
211 is introduced from the Mili-Q water. After that, the contamination from 85% H_3PO_4 with different
212 purity (acid-1: analytical reagent, AR; acid-2: High Performance Liquid Chromatography, HPLC)
213 are compared. The carbon contents in the 85% H_3PO_4 dissolved in Mili-Q water are 0.03-0.04 $\mu\text{g C}$
214 and show no significant discrepancy between different purity.

215 Interestingly, the carbon content increase to 0.5-0.6 $\mu\text{g C}$ after the persulfate is added,
216 implicating that the CO_2 in the procedural blank is mainly produced from the oxidation of organic
217 substance in the persulfate. The carbon content in HPLC grade of 85% H_3PO_4 mixed with the
218 persulfate (0.58 - 0.63 $\mu\text{g C}$) is closed to that of AR grade (0.46 - 0.63 $\mu\text{g C}$, see table 1.). Thus, AR
219 grade with purity of 85 % H_3PO_4 is utilized to prepare the oxidizing solution in this method. The
220 average carbon content of the procedural blank is estimated to be $0.5 \pm 0.06 \mu\text{g C}$, and the detection
221 limit is expected to be 10 times the procedural blank (i.e. 5 $\mu\text{g C}$). The carbon content in the
222 procedural blank of this method is much lower than that of the methods analyzing isotopes of WSOC
223 in aquatic environment or soil (De Groot, 2004; Polissar et al., 2009; Werner et al., 1999). The
224 smaller carbon content of the procedural blank suggests the possibility to correctly measure the
225 WSOC and $\delta^{13}\text{C}_{\text{WSOC}}$ of samples containing low carbon content.

226 3.2 Flushing methods

227 To avoid any contamination, the headspace of the sample vial has to be flushed with the high-
228 purity helium to remove the CO_2 (both dissolved and gas phase). Two different flushing methods
229 (F1 and F2) are compared here. F1 is a one-step flushing: helium is bubbled under the water surface
230 for 5 min in a sealed vial, and the gas in the headspace is released through a stainless steel tube to
231 the atmosphere. The open end of this tube is submerged in Milli-Q water to balance the air pressure
232 and to prevent any backflow of the atmospheric CO_2 . F2 requires two steps: the helium is first
233 bubbled under the water surface for 5 min in an open vial to remove the dissolved CO_2 in the solution.
234 After the vial is sealed, the helium is flushed again into the headspace for 5 min by piercing the

235 septum with a two-hole sample needle. The two holes are performed as the inlet of the helium and
236 the exit of the outflow, respectively. Since the flow rate of the inlet helium is larger than that of the
237 outflow, the headspace pressure is considered to be greater than 1atm. In that case, the most
238 noticeable difference between F1 and F2 is the air pressure of the headspace.

239 Different concentrations of working standard (KHP) are tested to compare the flushing
240 methods. The results obtained from F1 and F2 show no significant difference regardless of the
241 concentration of KHP. This represents that F1 and F2 are both able to completely remove the CO₂
242 in the vials. But it has to be noticed that F2 produces excessive air pressure in the headspace, the
243 following heating step may increase the risk of gas leak. Gas leaking during the preparation usually
244 results in the loss of carbon content and the isotope fractionation. Besides, flushing with F2 takes 5
245 more minutes for each sample compared with F1. Consequently, F1 is considered as the suitable
246 flushing method to remove CO₂ dissolved in the solution and the headspace.

247 3.3 Heating time

248 In order to assure the complete oxidation of WSOC, duration time for heating the samples is
249 tested with KHP, a widely used WSOC standard which is difficult to oxidize. Figure 2 shows the
250 carbon contents and the $\delta^{13}\text{C}$ values of KHP solutions heated from 15 min to 120 min at 100°C.
251 Some caps of the sample vials are out of shape after heating for longer time (more than 60 min),
252 suggests gas leak of the vials. High pressure can be built up in the headspace with the increase of
253 the temperature during the long time heating, especially for the vials containing more carbon
254 contents. The CO₂ gas produced in the headspace may leak through the minor holes on the septum
255 pierced by the stainless tube during the helium flushing step (step 5 in Fig 1.). According to the
256 kinetic isotope effect (KIE), isotope fractionation occurs during the gas leaking. The light carbon
257 isotopes (¹²C) are easier to escape from the vials than the heavy ones (¹³C), thus the remaining CO₂
258 would be more enriched with heavy isotopes (¹³C). In that case, lower carbon contents and higher
259 $\delta^{13}\text{C}$ values are expected to be observed in the results of leaking vials. In the results of the KHP
260 standards, some of the vials containing larger amount of organic carbon are detected to have
261 extremely low carbon contents corresponding with very high isotopic ratios. For example, one of
262 the 10 $\mu\text{g C}$ KHP standard is measured to be 1.2 $\mu\text{g C}$ and $\delta^{13}\text{C} = 14.9\text{‰}$ after 120 min of heating;
263 one of the 30 $\mu\text{g C}$ KHP standard is measured to be 2.4 $\mu\text{g C}$ and $\delta^{13}\text{C} = 17.7\text{‰}$ after 90 min of
264 heating (Fig. 2.). The stable results (both carbon contents and the isotopes, Fig. 2.) of 4 $\mu\text{g C}$

265 standards are probably due to the less CO₂ gas and lower pressure produced in the headspace during
266 the heating. Accordingly, heating time longer than 60 min increases the probability of gas leak in
267 the measurement.

268 In the aspect of the isotope composition, KHP standards heated for 15min, 30min and 60 min
269 all show stable results with similar standard deviations (from 0.51 - 0.57, see Table S1). While, the
270 heating time of 15min and 30 min are not long enough for the complete oxidation, which is shown
271 in lower carbon contents (Fig. 2.). Therefore, heating for 60 min at 100°C is found to be the most
272 suitable to produce constant results without gas leak and isotope fractionation.

273 3.4 Waiting time and instrument settings

274 The waiting time of the mixture (the aerosol extract and the oxidizing solution) between step 4
275 and 5 in Fig. 1. is tested to prevent the CO₂ loss during the flushing. Some of the compounds in
276 aerosol samples could be oxidized at room temperature. The CO₂ generated from the mixture before
277 heating could be lost during the flushing step (Sharp, 1973). The ambient sample is tested to detect
278 the room - temperature - oxidized CO₂ (Fig. S1.). Replicates of the ambient aerosol extract (from
279 one filter) are mixed with the oxidizing solution, and the mixtures of the aerosol extract and the
280 oxidizing solution are flushed with He to exclude the effect of CO₂ (both in the headspace and in
281 the mixture) as soon as possible. After flushing, the mixtures are stored at room temperature from
282 1 to 31 hours before analysis without heating. The carbon contents produced in the mixtures that
283 stored less than 12 h before analysis is smaller than 0.02 µg, which contributes to ~ 7% to the carbon
284 content in the procedural blank (0.5µg C). But when the waiting time is extended to 31 h, up to 2.3
285 µg C (about 5 times of the procedural blank) is oxidized into CO₂. The room - temperature - oxidized
286 CO₂ produced during the waiting time would be flushed out by the He in the later procedure and
287 then would result in significant isotope fractionation in the delta results. Therefore, the mixture
288 should be flushed with He within 12 h to avoid the CO₂ loss and isotope fractionation.

289 In addition, various combinations of shorter loading times (30-90 s) and/or fewer sample peaks
290 (i.e. 5 sample peaks) are tested with reference gas (CO₂ mixed with He) to shorten the analysis in
291 the system. However, the amount of CO₂ in the reference gas detected by the mass spectrometry is
292 about 2 µg C lower compared the results obtained with longer loading times and more sample peaks.
293 And there is a decrease of isotope value (~ 0.4 ‰) as well when the loading time is shorter or the

294 sample peaks are less than 10. Thus, 120 s loading time and 10 sample peaks are necessary for the
295 precise results, and the standard deviation is < 0.03 % for the 10 sample peaks within a run.

296 3.5 Calibration of the results

297 3.5.1 Quantification of the carbon content

298 The sample peak area is proportional to the carbon content in the vial and then is used to
299 quantify the amount of CO₂ in the inflow of IRMS. The average value of the peak areas for the last
300 eight sample peaks is taken as the peak area of a certain sample. The first two sample peaks are
301 excluded to avoid the effect of the residual CO₂ of the former vial. We established a carbon content
302 standard curve (linear equation) by measuring the peak areas of CO₂ gas samples containing 1-24
303 µg C (Fig. S2.). It has to be noted that the gas samples containing larger carbon contents are not
304 tested for the difficulty of injecting too much volume of CO₂/He gas. Then the amount of CO₂
305 oxidized from the unknown samples can be quantified with this linear equation (i.e., Carbon content
306 (µg) = Peak area (Vs) × (2.50 ± 0.08) – (0.62 ± 0.39), R²=0.98). The standard curve (linear equation)
307 of the peak areas against the carbon contents in the WSOC solution (KHP solution containing 1-100
308 µg C) is also established (Fig. S2.). And a linear equation similar with the peak areas against CO₂
309 gas is obtained (i.e., Carbon content (µg) = Peak area (Vs) × (2.34 ± 0.01) – (0.86 ± 0.14), R²=1.00).

310 Then the conversion efficiency of the WSOC extract containing 1-100 µg C can be roughly
311 calculated as 104 ± 3 %. The high conversion efficiency demonstrates the completely conversion
312 and the negligible isotope fractionation during the oxidation. In that case, the carbon content in the
313 WSOC extract of unknown samples can be calculated based on the standard curve of peak areas
314 against the carbon content in the WSOC extract. And the standard curve quantifying the carbon
315 content has to be established with every batch of unknown samples to assure the completely
316 conversion.

317 3.5.2 Blank correction

318 The blank contribution to the WSOC mass concentrations and the δ¹³C_{WSOC} values are
319 evaluated with the peak area and the isotope value of the procedural blank. The peak area (average
320 value of the last eight peaks) from the measurement is proportional to the carbon content in the vial
321 and then is taken to represent the CO₂ amounts in the inflow of IRMS. The procedural blank can be
322 corrected according to the mass balance as follows.

323
$$\delta^{13}C_{meas} \times A_{meas} = \delta^{13}C_{corr} \times (A_{meas} - A_{blk}) + \delta^{13}C_{blk} \times A_{blk} \quad (1)$$

324 Where $\delta^{13}C_{corr}$, $\delta^{13}C_{meas}$ and $\delta^{13}C_{blk}$ are the blank-corrected $\delta^{13}C$, the measured $\delta^{13}C$ of the samples
 325 and the $\delta^{13}C$ of the procedural blank, respectively. A_{meas} and A_{blk} denote the peak areas of the
 326 samples and the blank, correspondingly.

327 In order to calibrate the contribution of the procedural blank to the isotope results, A_{blk} and
 328 $\delta^{13}C_{blk}$ are calculated with an indirect method (Polissar et al., 2009). KHP ($\delta^{13}C = -30.40\text{‰}$) and
 329 CH_6 ($\delta^{13}C = -12.20\text{‰}$) with various concentrations are measured to calculate A_{blk} and $\delta^{13}C_{blk}$. The
 330 wide range of their isotopes can basically cover the $\delta^{13}C_{wsoc}$ values in most ambient aerosol
 331 samples. According to Eq. (1), $\delta^{13}C_{meas}$ can be written as the following:

332
$$\delta^{13}C_{meas} = \delta^{13}C_{corr} + A_{blk}(\delta^{13}C_{blk} - \delta^{13}C_{corr})/A_{meas} \quad (2)$$

333 According to Eq. (2), there is a linear relationship of the $\delta^{13}C_{meas}$ values and the reciprocal of
 334 peak areas ($1/A_{meas}$). Based on the keeling plot theory, linear equations of the $\delta^{13}C_{meas}$ values and
 335 $1/A_{meas}$ for the two standards can be set up separately (e.g., $\delta^{13}C$ and $1/A_{meas}$ values obtained from
 336 the measurement of CH_6 and their linear relationship are shown in Fig.S3.). The slopes (k_1 and k_2)
 337 and the intercepts (b_1 and b_2) of this liner relationship can be expressed with $\delta^{13}C_{blk}$, A_{blk} and $\delta^{13}C_{corr}$
 338 as follows.

339
$$\begin{aligned} k_1 &= A_{blk} \times (\delta^{13}C_{blk} - \delta^{13}C_{corr-std1}) \\ k_2 &= A_{blk} \times (\delta^{13}C_{blk} - \delta^{13}C_{corr-std2}) \end{aligned} \quad (3)$$

340
$$\begin{aligned} b_1 &= \delta^{13}C_{corr-std1} \\ b_2 &= \delta^{13}C_{corr-std2} \end{aligned} \quad (4)$$

341 Thus, A_b and $\delta^{13}C_b$ can be calculated as follows:

342
$$\delta^{13}C_{blk} = (k_2 \times b_1 - k_1 \times b_2)/(k_2 - k_1) \quad (5)$$

343
$$A_{blk} = (k_2 - k_1)/(b_1 - b_2) \quad (6)$$

344 Thus, the blank contribution is able to be calibrated with the equation below:

345
$$\delta^{13}C_{corr} = (\delta^{13}C_{meas} \times A_{meas} - \delta^{13}C_{blk} \times A_{blk})/(A_{meas} - A_{blk}) \quad (7)$$

346 For example, $\delta^{13}C_{blk}$ and A_{blk} are calculated to be -27.43‰ and $0.3Vs$ ($\sim 0.5 \mu\text{g C}$) based on the
 347 results of KHP and CH_6 (shown in Fig. 3.). The carbon content in the procedural blank contributes
 348 to 1 – 10% carbon content of an ambient aerosol sample. Although the $\delta^{13}C_{blk}$ and A_{blk} are not
 349 strongly varied values, they need to be measured before every batch of the ambient samples to assure
 350 the stable status of the system (IRMS) and the proper processes during the pretreatment.

351 3.5.3 Calibration of isotope results

352 In order to calibrate the isotope results, four working standards (KHP, BA, CH₆ and C₂)
353 containing different carbon contents are measured with EA-IRMS and Gas Bench II-IRMS. The
354 standards measured with EA are combusted at 1000°C to convert the organic materials into CO₂ for
355 the measurement in IRMS without pretreatment. More than 10 repetitions of each standard are
356 measured in this way, the average delta values (after blank correction) of each standard are defined
357 as correct values here. On the other hand, the average isotope compositions (after blank correction)
358 of 10 repetitions obtained from the wet oxidation method (determined with Gas Bench II) are
359 defined as measured values. Thus the calibration curve can be established on the basis of the
360 measured values and the correct values (Fig. S4.). For instance, the isotope results can be calibrated
361 as follows:

$$362 \quad \delta^{13}C_{cali} = k \times \delta^{13}C_{blk-corr} + b \quad (8)$$

363 $\delta^{13}C_{cali}$ is the isotope composition after the isotope calibration, $\delta^{13}C_{blk-corr}$ is the blank corrected
364 isotope composition determined with Gas Bench II, k and b are the slope and the intercept obtained
365 from the calibration curve. Similar with the blank correction, the isotope calibration curve needs to
366 be established with each batch of the ambient samples to assure the stable status of the IRMS and
367 the proper processes during the pretreatment.

368 In this way, the isotope results can be calibrated, the raw data and the isotope composition after
369 the blank correction and the isotope calibration determined with Gas Bench II are compared in Fig.
370 3. The correct values of standard carbon isotopes are plotted in Fig. 3. as well. The isotope results
371 after two steps of correction (the blank correction and the calibration of isotope results) are closer
372 to the correct values (isotopes measured with EA) and the blank contribution are drastically
373 eliminated. But as for the standards containing carbon content smaller than 5 $\mu\text{g C}$, the contribution
374 of the procedural blank (with an isotope ratio about -27.43‰) is still significant. According to the
375 isotope variation of the ambient aerosols, the analysis of isotope compositions is not reliable if the
376 repetitions of the standards show difference larger than 1‰ (SD > 0.5 ‰). After correction, the
377 standard deviations of isotope results of each standard are better than 0.17 ‰ (regardless of the
378 carbon content of a certain standard) when the carbon contents are larger than 5 $\mu\text{g C}$. In that case,
379 the detection limit of this method is 5 $\mu\text{g C}$ and the results (both carbon contents and the isotopic
380 ratios) of WSOC lower than 5 $\mu\text{g C}$ were not reliable.)

381 3.6 QA/QC procedure

382 A batch of working standards with different carbon contents are measured to evaluate the
383 optimized method in this study (data shown in Fig. 3.). The quality of the unknown samples is
384 assured with a standard curve established with the peak areas and the corresponding input carbon
385 contents of WSOC extract (e.g. in Fig. S2.). The conversion efficiency of the WSOC oxidation is
386 $104 \pm 3\%$. The average recovery of the working standards and the ambient samples are tested to be
387 $97 \pm 6\%$ and $99 \pm 10\%$, respectively. The conversion efficiency and the recoveries suggest
388 completely oxidation of WSOC extract without significant isotope fractionation in the pretreatment.
389 The blank contribution is evaluated with the peak area and the isotopic ratio, these values are
390 calculated with the indirect method introduced in Sect. 3.5.2. According to the carbon content (0.3
391 $- 0.5 \mu\text{g C}$) and the isotope composition ($\sim -27.43\text{‰}$) of the procedural blank, the WSOC detection
392 limit of this method is $5 \mu\text{g C}$, 10 times of the carbon content in the procedural blank. The blank
393 corrected isotope compositions should be calibrated again with the calibration curve as described in
394 Sect. 3.5.3 to obtain the isotopic ratios of the unknown samples.

395 In order to obtain the carbon contents and the corrected isotope compositions of the unknown
396 samples, at least two kinds of standards need to be measured before every batch of the unknown
397 samples. The range of the carbon contents and the isotope compositions of the standards are required
398 to cover the range of WSOC and $\delta^{13}\text{C}_{\text{WSOC}}$ in the ambient samples, e.g. KHP, BA and CH_6 . Hence,
399 the concentration standard curve, the linear equations for the blank correction and the isotope
400 calibration curve are able to be established according to the results of the standards. Besides, one
401 standard should be measured after every 10 unknown samples to assure the stable status of the
402 equipment.

403 As for the isotope measurement, the precision of the last eight sample peaks is $< 0.15\text{‰}$ within
404 a run for standards containing more than $1 \mu\text{g C}$; between runs, the deviation of the standards with
405 different carbon contents ($> 5 \mu\text{g C}$, $n \geq 10$) is $< 0.17\text{‰}$. The accuracy is estimated to be better than
406 0.5‰ by comparing the calibrated $\delta^{13}\text{C}$ results from Gas Bench II and the blank corrected isotopic
407 ratios from EA. Isotope results tested by Gas Bench II is slightly lower compared to the results of
408 EA. The ambient aerosol filters are tested repeatedly to evaluate the reproducibility of the ambient
409 samples as well. The standard deviation of the WSOC concentrations and the isotope results of the
410 repeated ambient samples are $0.25 \pm 0.04 \mu\text{g C}$ ($n \geq 3$) and $0.14 \pm 0.07\text{‰}$ ($n \geq 3$), respectively. To

411 conclude, the presented method is considered to be precise and accurate to detect the low abundance
412 of WSOC as well as isotopes in aerosol samples.

413 To test the applicability of this method measuring the atmospheric WSOC, the ambient aerosol
414 samples collected in Nanjing are analyzed. And the WSOC concentrations are measured with TOC
415 analyzer (Shimadzu) for comparison. Figure 4. shows the scattered plot of WSOC concentrations
416 measured with the two peripherals (TOC analyzer and Gas Bench II-IRMS). The strong correlation
417 ($R^2 = 0.95$, $p < 0.01$) and the slope (0.97) demonstrate the reliability of measuring WSOC with the
418 presented method. It suggests complete oxidation of WSOC in aerosol samples, which means no
419 significant carbon isotope fractionation happens during the preparation. Moreover, the $\delta^{13}\text{C}_{\text{-WSOC}}$
420 values (between -26.24‰ to -23.35‰) of ambient aerosols are close to the published data (from -
421 26.5‰ to -17.5‰) (Kirillova et al., 2013; Kirillova et al., 2014). In that case, the $\delta^{13}\text{C}$ values
422 resulted from this method are considered to be effective for ambient WSOC.

423 **4. Sources and atmospheric processes of WSOC**

424 4.1 Temporal variation

425 Time series of $\text{PM}_{2.5}$, $\delta^{13}\text{C}$ values, chemical tracers and meteorological data observed at the
426 sampling site during the studied period are illustrated in Fig. 5. WSOC ranges from 3.0 to $32.0\ \mu\text{g}\ \text{m}^{-3}$,
427 occupying $49 \pm 10\%$ of total carbon in $\text{PM}_{2.5}$. The stable carbon isotopes of WSOC and TC
428 vary between -26.24‰ to -23.35‰ and -26.83‰ to -22.25‰ , respectively. $\delta^{13}\text{C}$ values shift over
429 2‰ in 24 hours, and over 1‰ in 3 hours, which is not able to be captured in lower time resolution
430 samples (e.g., 12h or 24h). In that case, this data set can be interpreted with more detailed
431 information about the WSOC sources and the atmospheric processes. Biomass burning tracer (nss-
432 K^+), dust tracer (Ca^{2+}), MODIS fire spots and air mass trajectories are analyzed to investigate the
433 potential sources of WSOC. Nss- K^+ is used as a proxy of biomass burning (Zhang et al., 2013). Nss-
434 K^+ concentrations are evaluated from Na^+ concentrations in the samples according to their
435 respective ratios ($\text{K}^+/\text{Na}^+=0.037\ w/w$) in seawater (Osada et. al., 2008).

$$436 \quad \text{nss} - \text{K}^+ = [\text{K}^+] - 0.037 \cdot [\text{Na}^+] \quad (9)$$

437 where $[\text{K}^+]$ and $[\text{Na}^+]$ are the total mass concentrations of K^+ and Na^+ of the aerosol samples.
438 The concentration of nss- K^+ ranges from 0.16 to $6.70\ \mu\text{g}\ \text{m}^{-3}$ with an average of $1.31\ \mu\text{g}\ \text{m}^{-3}$. The
439 high concentrations and the intense increase in Jan 24th indicate a significant biomass burning event
440 and will be discussed later.

441 As shown in Fig. 5., $\delta^{13}\text{C}_{\text{TC}}$ and $\delta^{13}\text{C}_{\text{WSOC}}$ show similar pattern during the sampling period. In
442 general, $\delta^{13}\text{C}_{\text{TC}}$ is slightly lower than $\delta^{13}\text{C}_{\text{WSOC}}$, and the trend is also observed elsewhere (Fisseha
443 et al., 2009). The difference is related to the sources and the atmospheric processes during the
444 formation and transformation of carbonaceous particles in the atmosphere. The C4 plants biomass
445 burning and the marine organic materials are the sources with relatively enriched ^{13}C . Smith and
446 Epstein (1971) suggest that C4 plants have a mean $\delta^{13}\text{C}$ isotope signature of -13 ‰. And the isotope
447 composition of carbon emitted from phytoplankton, an example of primary marine aerosol, is about
448 -22 ‰ to -18 ‰ (Miyazaki et al., 2011). However, January is not a specific time period for the
449 growing or combustion of C4 plants in East China, indicating small possibility of C4 plants biomass
450 burning as a major source of WSOC aerosols. In addition, both WSOC and non-WSOC components
451 can be emitted from biomass burning, thus the C4 plants combustion would generally result in the
452 enrichment of ^{13}C in both TC and WSOC. The air parcel transported from marine areas normally
453 has little effect on the aerosols during winter in Nanjing (Qin et al., 2016), suggesting the negligible
454 contribution of marine emissions to WSOC during the sampling period. Therefore, the WSOC
455 sources with higher isotope signatures (compared with non-WSOC sources) are not able to explain
456 the higher values of $\delta^{13}\text{C}_{\text{WSOC}}$ over $\delta^{13}\text{C}_{\text{TC}}$.

457 Apart from the sources, the secondary formation (Hecobian et al., 2010; Jimenez et al., 2009;
458 Saarikoski et al., 2008) of WSOC is reported to affect the isotope compositions. Precursors like
459 VOCs can be oxidized with the hydroxyl radicals and ozone to produce WSOC in the atmosphere
460 (Pathak et al., 2011). Laboratory and field studies demonstrate that the lighter isotopes have the
461 priority to be oxidized and produce particulates with lower isotopic ratios. For example, the
462 oxidation of VOCs in the atmosphere would result in the ^{13}C depletion in the products and the ^{13}C
463 enrichment in the residual VOCs (Rudolph et al., 2002). In other words, the secondary formation
464 tends to lower the $\delta^{13}\text{C}$ value of ambient WSOC, thus the secondary formation could not explain
465 the ^{13}C enrichment in WSOC compared to TC.

466 Studies demonstrate that the photochemical aging process during the long range transport
467 causes significant enrichment in ^{13}C . (Aggarwal and Kawamura, 2008; G. Wang et al., 2010). The
468 isotope fractionation is up to 3 ‰ - 7 ‰ of the residual during the photolysis of oxalic acid, a
469 dominant species in WSOC aerosols (Pathak et al., 2011). Due to the hydrophilic property, WSOC
470 is associated with the aerosol aging processes. WSOC/OC ratio is normally considered to represent

471 the aging status of aerosol samples (Agarwal et al., 2010; Pathak et al., 2011), it increases with the
472 photochemical aging process. The ratio of WSOC/OC is 0.67 ± 0.12 (Fig. S5.) in this study, which
473 is higher than the aged aerosols with WSOC/OC = 0.41 reported elsewhere (Huang et al., 2012).
474 The high ratio of WSOC/OC indicates aged aerosols during the sampling period. Thus the
475 photochemical aging process could partially explain the reason of higher values of $\delta^{13}\text{C}_{\text{-WSOC}}$
476 (compared with $\delta^{13}\text{C}_{\text{-TC}}$).

477 According to the principle of mass balance, ^{13}C depleted sources of non-WSOC can also result
478 in the depletion of ^{13}C in TC. TC is consist of OC, EC and carbonate carbon (CC) (Huang et al.,
479 2006), and OC can be divided into WSOC and water insoluble OC (WIOC) according to the
480 hydrophilic character (Eq. 10). In most circumstances, CC is negligible to the amount of TC in $\text{PM}_{2.5}$
481 (Huang et al., 2006; Ten Brink et al., 2004), thus non-WSOC component could be presented as Eq.
482 11.

$$483 \quad \text{TC} = \text{OC} + \text{EC} + \text{CC} = \text{WSOC} + \text{WIOC} + \text{EC} + \text{CC} \quad (10)$$

$$484 \quad \text{TC} - \text{WSOC} = \text{WIOC} + \text{EC} \quad (11)$$

485 WIOC and EC are generally originated from primary emissions (Park et al., 2013; Y. L. Zhang
486 et al., 2014), and the $\delta^{13}\text{C}$ values are better representing their sources. In that case, the ^{13}C depleted
487 source which only contributes to non-WSOC components, such as WIOC emitted from the
488 vegetation, is likely to be another reason of $\delta^{13}\text{C}_{\text{-TC}}$ depletion during the sampling period.

489 4.2 Three episodes

490 During the sampling period, three significant haze events (e.g., namely the Episode 1, the
491 Episode 2, the Episode 3) are observed in Nanjing. These 3 episodes show different tendencies of
492 $\delta^{13}\text{C}_{\text{-WSOC}}$ variation during the accumulation of WSOC aerosols (see Fig. 5.). The Episode 1 and 2
493 are compared here due to the distinct $\delta^{13}\text{C}_{\text{-WSOC}}$ trends with WSOC accumulation. In the Episode 3,
494 ^{13}C is found to be enriched in TC compared to WSOC ($\delta^{13}\text{C}_{\text{-WSOC}} < \delta^{13}\text{C}_{\text{-TC}}$, $p < 0.01$), in contrast to
495 the trend of isotope compositions during other periods ($\delta^{13}\text{C}_{\text{-WSOC}} > \delta^{13}\text{C}_{\text{-TC}}$, $p < 0.01$).

496 4.2.1 The Episode 1

497 As for the Episode 1, the $\delta^{13}\text{C}_{\text{-WSOC}}$ values increase with the mass concentrations of WSOC (r
498 = 0.84, $p < 0.001$, see Fig. 6d.), indicating the sampling site is impacted by ^{13}C enriched WSOC
499 sources and/or photochemical aged aerosols. As shown in Fig. 6a., air mass trajectories of WSOC
500 with higher $\delta^{13}\text{C}_{\text{-WSOC}}$ values ($>24\%$) are originated mainly from northern China, and the northerly

501 wind prevails at this site (Fig. 5g.). During the long-range transport, the studied WSOC mass
502 concentration increases with the ^{13}C enrichment of WSOC due to the isotope fractionation in the
503 photochemical aging process. This is supported by the increasing ratio of WSOC/OC (from 0.73 to
504 0.91) in the Episode 1 (Fig. S5.).

505 According to the higher isotopes ($\delta^{13}\text{C}_{\text{wsoc}} > -24\text{‰}$) and the corresponding trajectories (Fig.
506 6a.), C4 plants biomass burning ($\delta^{13}\text{C} \sim -12\text{‰}$, [Martinelli et al., 2002; Sousa Moura et al., 2008])
507 and coal combustion ($\delta^{13}\text{C} \sim -24.9\text{‰}$ to -21‰ , [Cao et al., 2011]) are considered to be possible
508 sources of WSOC. Nss-K^+ is largely originated from plants combustion (Zhang et al., 2013), and is
509 analyzed as a proxy of biomass burning. However, during this period the nss-K^+ level (0.56 ± 0.41
510 $\mu\text{g m}^{-3}$) is not significantly increased and is generally lower than the average value ($1.3 \mu\text{g m}^{-3}$,
511 Fig.5e), indicating that the C4 plants biomass burning is not a major source of WSOC. Besides, the
512 main crops growing in northern China are mainly C3 plants such as wheat and rice instead of C4
513 plants during the sampling period (Chen et al., 2004). And the biomass burning contribution of C3
514 plants would even lower the $\delta^{13}\text{C}$ values of WSOC. What's more, there are only few MODIS fire
515 spots along with the trajectories from northern China (Fig. 6a.). In that case, open field biomass
516 burning is not considered as a major source of WSOC at the sampling site during the Episode 1.

517 Furthermore, the WSOC mass concentrations and the $\delta^{13}\text{C}_{\text{wsoc}}$ values decrease synchronously
518 with the change of the wind direction (from north to southeast) after the Episode 1. The southeast
519 wind breaks the continuous transport of WSOC from northern China. And the relatively lower $\delta^{13}\text{C}_{\text{wsoc}}$
520 values are then observed, suggesting a regional isotope signal of WSOC without the substantial
521 aging. Besides, the WSOC/OC declines obviously with the isotope after the Episode 1 (Fig. S5.),
522 indicating less contribution of aged aerosols to the sampling site. Therefore, the elevated $\delta^{13}\text{C}_{\text{wsoc}}$
523 values with the increased WSOC mass concentrations in the Episode 1 are mainly affected by the
524 aged aerosols transported from northern China.

525 4.2.2 The Episode 2

526 The $\delta^{13}\text{C}_{\text{wsoc}}$ values show an opposite trend with WSOC mass concentrations ($r = -0.54$, $p <$
527 0.01 , see Fig. 6e.) in the Episode 2. At the beginning of the Episode 2 (Jan 22nd), the sampling site
528 is mainly affected by the air mass from the north of Nanjing, and the WSOC displays with relatively
529 higher $\delta^{13}\text{C}_{\text{wsoc}}$ values at the same time (Fig. 6b). After Jan 22nd, the shift of the wind direction
530 and the air mass trajectories are well corresponded with the decline of the $\delta^{13}\text{C}_{\text{wsoc}}$ values (Fig.

531 6b.). The large amount of fire spots in the potential source regions suggests the significant impact
532 of open field biomass burning. It should be noted that the stable carbon isotope composition of C3
533 plants combustion is relatively low (i.e., $\delta^{13}\text{C} \sim -27\%$, [Martinelli et al., 2002; Sousa Moura et al.,
534 2008]). The $\delta^{13}\text{C}_{\text{WSOC}}$ values decrease and the WSOC mass concentrations peak to the maximum
535 when the air mass travels throughout the regions with a great many hot spots. The concentration of
536 nss-K^+ has a positive correlation with WSOC concentration ($r = 0.82$, $p < 0.001$) and a negative
537 correlation with $\delta^{13}\text{C}_{\text{WSOC}}$ ($r = -0.45$, $p < 0.05$) during the Episode 2. And the concentration of nss-
538 K^+ increases up to $6.7 \mu\text{g m}^{-3}$, about 7 times of the average value, indicating a significant biomass
539 burning contribution (Fig. 5e). The decrease of the $\delta^{13}\text{C}_{\text{WSOC}}$ values and the increase of the biomass
540 burning tracers (i.e., nss-K^+) suggest that the biomass burning emission is a major contribution of
541 WSOC aerosols. Also, the WSOC/OC ratio declines from 0.88 to 0.53 (Fig. S5.), indicating that the
542 increased WSOC is rather from fresh biomass-burning aerosols without a substantial aging process.

543 4.2.3 The Episode 3

544 The ^{13}C is clearly enriched ($p < 0.01$) in TC ($-23.5 \pm 0.43 \%$) compared to WSOC ($-25.17 \pm$
545 1.08%) during the Episode 3 (see Fig. 6f.). This might be related with a ^{13}C -enriched source and/or
546 the aging process of non-WSOC fraction in TC. Non-WSOC fraction is mainly consist of WIOC,
547 EC and carbonate carbon (CC). Among these carbonaceous species, carbonate carbon (CC) exhibits
548 with much higher $\delta^{13}\text{C}$ values than EC and OC (Kawamura et al., 2004). CC could be a significant
549 fraction of dust aerosols, even though it is a very small part of TC in $\text{PM}_{2.5}$ in most cases.

550 To study the dust contribution in the Episode 3, Ca^{2+} is determined as an indicator of dust
551 (Huang et al., 2010; Jankowski et al., 2008). Ca^{2+} and TC show similar patterns ($R^2 = 0.84$, $p < 0.01$),
552 indicating dust origins in this period. The argument is also supported by the 48-h backward
553 trajectory analysis (Fig. 6c.). It shows that the air mass is mainly originated from a semi-arid region,
554 Mongolia. The photochemical aging of dust aerosols during the long-range transport from Mongolia
555 to Nanjing could possibly promotes the ^{13}C enrichment. For short, the enrichment of ^{13}C in TC over
556 WSOC is due to a dust event transported to the studied site.

557 According to the mass balance, the isotopic ratio of TC affected by CC in the dust aerosols can
558 be expressed as follows:

$$559 \quad \delta^{13}\text{C}_{\text{TC}} = f_{\text{CC}} \times \delta^{13}\text{C}_{\text{CC}} + (1 - f_{\text{CC}}) \times \delta^{13}\text{C}_{\text{NC}} \quad (12)$$

560 where the $\delta^{13}\text{C}_{\text{-TC}}$, $\delta^{13}\text{C}_{\text{-CC}}$ and $\delta^{13}\text{C}_{\text{-NC}}$ are the measured stable carbon isotope of TC, the isotopic
561 ratio of CC in dust aerosols and the isotope composition of non-CC fractions. The f_{cc} represents the
562 CC contribution to TC. The CC contribution during the Episode 3 is roughly estimated based on a
563 few assumptions: 1) the increase of TC and $\delta^{13}\text{C}_{\text{-TC}}$ is only affected by the dust origin, 2) the average
564 value of $\delta^{13}\text{C}_{\text{-TC}}$ (-25 ‰) during the studied period (except the Episode 3) is taken as the value of
565 $\delta^{13}\text{C}_{\text{-NC}}$, 3) $\delta^{13}\text{C}_{\text{-CC}} = 0.3$ ‰ in dust sources (Kawamura et al., 2004). With these considerations, CC
566 contribution is estimated to contribute up to 10% to TC according to the Eq. 12.

567 **5. Conclusions**

568 An optimized method for the determination of WSOC mass concentrations and $\delta^{13}\text{C}_{\text{-wsoc}}$
569 values in aerosol samples with Gas Bench II - IRMS is presented. A two-step correction is applied
570 to correct the blank contribution and to calibrate the isotope results. The procedural blank is
571 estimated to be 0.5 $\mu\text{g C}$ with isotope composition of -27.43 ‰. The detection limit is demonstrated
572 to be 5 $\mu\text{g C}$ according to the measurement of working standards with various carbon contents. The
573 method yields a high recovery of the standards (97 ± 6 %) and ambient samples (99 ± 10 %).
574 According to the high recoveries, the isotope fractionation during the pretreatment is tend to be
575 negligible. The precision and the accuracy is better than 0.17 ‰ and 0.5 ‰, separately. WSOC
576 concentrations determined with this optimized method is consistent ($R^2 = 0.95$) with the results of
577 the TOC analyzer. Compared with the previous methods, the optimized method presented in this
578 study is more precise and accurate, and requires less time-consuming pretreatment.

579 The presented method is then applied to analyze the $\delta^{13}\text{C}_{\text{-wsoc}}$ of the high time resolution
580 aerosol samples collected during a severe winter haze in East China. WSOC ranged from 3.0 $\mu\text{g m}^{-3}$
581 to 32.0 $\mu\text{g m}^{-3}$, and $\delta^{13}\text{C}_{\text{-wsoc}}$ varies between -26.24 ‰ to -23.35 ‰. ^{13}C is more enriched in WSOC
582 than TC in the majority of the sampling period, indicating aged aerosols and/or ^{13}C depleted primary
583 sources of non-WSOC component. Three haze events (e.g., namely the Episode 1, the Episode 2,
584 the Episode 3) are identified with different tendencies of $\delta^{13}\text{C}_{\text{-wsoc}}$ during the accumulation of
585 WSOC aerosols. Similar patterns of the WSOC concentrations and the $\delta^{13}\text{C}_{\text{-wsoc}}$ values in the
586 Episode 1 are demonstrated to be affected by the air mass transported from northern China. The
587 increase of $\delta^{13}\text{C}_{\text{-wsoc}}$ indicates that the WSOC aerosols from the studied site is subject to a
588 substantial photochemical aging process during the long range transport. The contrasting trend of
589 the WSOC and $\delta^{13}\text{C}_{\text{-wsoc}}$ values in the Episode 2 is interpreted as the contribution of regional C3

590 plants biomass burning sources. In the Episode 3, the heavier isotope (^{13}C) is clearly enriched in
591 total carbon (TC) compares to WSOC fraction due to the dust contribution.

592 The optimized method is demonstrated to be accurate and precise to detect the WSOC mass
593 concentration and its isotope compositions ($\delta^{13}\text{C}_{\text{WSOC}}$) in aerosols. Our results indicate that the high
594 time-resolved measurement of $\delta^{13}\text{C}_{\text{WSOC}}$ can be used to distinguish different atmospheric processes
595 such as photochemical aging and aerosol sources (e.g., biomass burning and dust). However, a
596 quantitative understanding of sources and formation processes of WSOC aerosols is still of great
597 challenge. To reduce the knowledge gaps, a combination of multiple methodologies is needed in
598 future studies, such as high time-resolved measurement of radiocarbon (^{14}C) and stable carbon
599 isotope compositions ($\delta^{13}\text{C}$), and the real-time measurement of chemical compositions (e.g.,
600 Aerosol Mass Spectrometers, AMS or Thermal Desorption Aerosol Gas Chromatograph-AMS).

601

602 **Author contributions.** YZ conceived and designed the study; YZ, FC and WZ designed the
603 experimental strategy; WZ and YX performed the sampling and isotope measurements; YZ and WZ
604 analyzed the experimental data; YZ and WZ proposed the hypotheses; WZ wrote manuscript with
605 YL; all other co-authors contributed to writing.

606

607 **Competing interests.** The authors declare that they have no competing interests.

608

609 **Acknowledgements.** This study is supported by the National Natural Science Foundation of China
610 (Grant nos. 91644103, 41761144056, 41603104), the National Key Research and Development
611 Program of China (Grant no. 2017YFC0212704) and the Provincial Natural Science Foundation of
612 Jiangsu (Grant no. BK20180040).

613

614 **Reference:**

615 Agarwal, S., Aggarwal, S. G., Okuzawa, K., and Kawamura, K.: Size distributions of dicarboxylic
616 acids, ketoacids, α -dicarbonyls, sugars, WSOC, OC, EC and inorganic ions in atmospheric
617 particles over Northern Japan: Implication for long-range transport of Siberian biomass
618 burning and East Asian polluted aerosols. *Atmospheric Chemistry and Physics*, 10(13), 5839–
619 5858. <https://doi.org/10.5194/acp-10-5839-2010>.

620 Aggarwal, S. G., and Kawamura, K.: Molecular distributions and stable carbon isotopic
621 compositions of dicarboxylic acids and related compounds in aerosols from Sapporo, Japan:
622 Implications for photochemical aging during long-range atmospheric transport. *Journal of*

623 Geophysical Research Atmospheres, 113(14), 1–13. <https://doi.org/10.1029/2007JD009365>,
624 2008.

625 Anderson, C., Dibb, J. E., Griffin, R. J., and Bergin, M. H.: Simultaneous measurements of
626 particulate and gas-phase water-soluble organic carbon concentrations at remote and urban-
627 influenced locations. *Geophysical Research Letters*, 35(13), 2–5.
628 <https://doi.org/10.1029/2008GL033966>, 2008.

629 Atkinson, R.: Kinetics and Mechanisms of the Gas-Phase Reactions of the Hydroxyl Radical with
630 Organic Compounds under Atmospheric Conditions. *Chemical Reviews* 86(1), 69–201.
631 <https://doi.org/10.1021/cr00071a004>, 1986.

632 Bao, M., Cao, F., Chang, Y., Zhang, Y. L., Gao, Y., Liu, X., Zhang Y. Y., Zhang W. Q., Tang T.
633 R., Xu Z. F., Liu S. D., Lee X. H., Li J., Zhang G.: Characteristics and origins of air pollutants
634 and carbonaceous aerosols during wintertime haze episodes at a rural site in the yangtze river
635 delta, china. *Atmospheric Pollution Research*, 8(5), 900-911,
636 <https://10.1016/j.apr.2017.03.001>, 2017

637 Bauer, J. E., Haddad, R. I., Des Marais, D. J.: Method for determining stable isotope ratios of
638 dissolved organic carbon in interstitial and other natural marine waters. *Marine chemistry*,
639 33(4): 335-351, [https://doi.org/10.1016/0304-4203\(91\)90076-9](https://doi.org/10.1016/0304-4203(91)90076-9), 1991.

640 Bozzetti, C., El Haddad, I., Salameh, D., Daellenbach, K. R., Fermo, P., Gonzalez, R., Minguillón,
641 M. C., Iinuma, Y., Poulain, L., Elser, M., Müller, E., Slowik, J. G., Jaffrezo, J. L.,
642 Baltensperger, U., Marchand, N., and Prévôt, A. S. H.: Organic aerosol source apportionment
643 by offline-AMS over a full year in Marseille, *Atmos. Chem. Phys.*, 17, 8247-8268, 2017a.

644 Bozzetti, C., Sosedova, Y., Xiao, M., Daellenbach, K. R., Ulevicius, V., Dudoitis, V., Mordas, G.,
645 Byčenkienė, S., Plauškaitė, K., Vlachou, A., Golly, B., Chazeau, B., Besombes, J. L.,
646 Baltensperger, U., Jaffrezo, J. L., Slowik, J. G., El Haddad, I., and Prévôt, A. S. H.: Argon
647 offline-AMS source apportionment of organic aerosol over yearly cycles for an urban, rural,
648 and marine site in northern Europe, *Atmos. Chem. Phys.*, 17, 117-141, 2017b.

649 Cai, Z., Jiang, F., Chen, J., Jiang, Z., and Wang, X.: Weather Condition Dominates Regional PM_{2.5}
650 Pollutions in the Eastern Coastal Provinces of China during Winter, Egu General Assembly
651 Conference.969–980. <https://doi.org/10.4209/aaqr.2017.04.0140>, 2018.

652 Cao, J.J., Chow, J.C., Tao, J., Lee, S.C., Watson, J.G., Ho, K.F., Wang, G.H., Zhu, C.S. and Han,
653 Y.M.: Stable carbon isotopes in aerosols from Chinese cities: Influence of fossil fuels.
654 *Atmospheric Environment*, 45(6), 1359–1363.
655 <https://doi.org/10.1016/j.atmosenv.2010.10.056>, 2011.

656 Chen, X.P., Zhou J.C., Wang X. R., Blackmer A. M., & Zhang F.: Optimal rates of nitrogen
657 fertilization for a winter wheat-corn cropping system in northern china. *Commun Soil Sci Plan*,
658 35(3-4), 583-597, <http://10.1081/CSS-120029734>, 2004.

659 Currie, L. A., Klouda, G. A., Benner, B. A., Garrity, K., Eglinton, T. I.: Isotopic and molecular
660 fractionation in combustion; three routes to molecular marker validation, including direct
661 molecular ‘dating’ (GC/AMS). *Atmospheric Environment*, 33(17):2789-2806,[http://doi:](http://doi:10.1016/S1352-2310(98)00325-2)
662 10.1016/S1352-2310(98)00325-2, 1999.

663 Das, O., Wang, Y., Hsieh, Y. P.: Chemical and carbon isotopic characteristics of ash and smoke
664 derived from burning of C and C grasses. *Organic Geochemistry*, 41(3):263-269,
665 <http://doi:10.1016/j.orggeochem.2009.11.001>, 2010.

666 De Groot, P. A.: Handbook of stable isotope analytical techniques (Vol. 1). Elsevier, 2004. Decesari,
667 S., Mircea, M., Cavalli, F., Fuzzi, S., Moretti, F., Tagliavini, E., and Facchini, M. C.: Source
668 attribution of water-soluble organic aerosol by nuclear magnetic resonance spectroscopy.
669 Environmental Science and Technology, 41(7), 2479–2484. <https://doi.org/Doi>
670 10.1021/Es0617111, 2007.

671 Fisseha, R., Saurer, M., Jäggi, M., Siegwolf, R.T., Dommen, J., Szidat, S., Samburova, V. and
672 Baltensperger, U.: Determination of primary and secondary sources of organic acids and
673 carbonaceous aerosols using stable carbon isotopes. Atmospheric Environment, 43(2), 431–
674 437. <https://doi.org/10.1016/j.atmosenv.2008.08.041>, 2009.

675 Fisseha R, Saurer M, Jäggi M, et al. Determination of stable carbon isotopes of organic acids and
676 carbonaceous aerosols in the atmosphere.[J]. Rapid Communications in Mass Spectrometry
677 Rcm, 2006, 20(15):2343-2347.

678 Fowler, K., Connolly, P. J., Topping, D. O., and O’Meara, S.: Maxwell–Stefan diffusion: a
679 framework for predicting condensed phase diffusion and phase separation in atmospheric
680 aerosol. Atmospheric Chemistry and Physics, 18(3), 1629–1642, 2018.

681 Gouw, J. A. D., Brock, C. A., Atlas, E. L., Bates, T. S., Fehsenfeld, F. C., & Goldan, P. D., Holloway
682 J. S., Kuster W. C., Lerner B. M., Matthew B. M., Middlebrook A. M., Onasch T. B., Peltier
683 R. E., Quinn P. K., Senff C. J., Stohl A., Sullivan A. P., Trainer M., Warneke C., Weber R. J.,
684 and Williams E. J.: Sources of particulate matter in the northeastern united states in summer:
685 1. direct emissions and secondary formation of organic matter in urban plumes. Journal of
686 Geophysical Research Atmospheres, 113(D8), D08301. <https://doi:10.1029/2007JD009243>,
687 2008. Hecobian, A., Zhang, X., Zheng, M., Frank, N., Edgerton, E. S., and Weber, R. J.: Water-
688 soluble organic aerosol material and the light-absorption characteristics of aqueous extracts
689 measured over the Southeastern United States. Atmospheric Chemistry and Physics, 10(13),
690 5965–5977. <https://doi.org/10.5194/acp-10-5965-2010>, 2010.

691 Huang, H., Ho, K.F., Lee, S.C., Tsang, P.K., Ho, S.S.H., Zou, C.W., Zou, S.C., Cao, J.J. and Xu,
692 H.M.: Characteristics of carbonaceous aerosol in PM_{2.5}: Pearl Delta River region,
693 China. Atmospheric research, 104, 227-236. <https://doi.org/10.1016/j.atmosres.2011.10.016>,
694 2012.

695 Huang, K., Zhuang, G., Li, J., Wang, Q., Sun, Y., Lin, Y., and Fu, J. S.: Mixing of Asian dust with
696 pollution aerosol and the transformation of aerosol components during the dust storm over
697 China in spring 2007. Journal of Geophysical Research, 115, D00K13.
698 <https://doi.org/10.1029/2009JD013145>, 2010.

699 Huang, L., Brook, J.R., Zhang, W., Li, S.M., Graham, L., Ernst, D., Chivulescu, A. and Lu, G.:
700 Stable isotope measurements of carbon fractions (OC/EC) in airborne particulate: A new
701 dimension for source characterization and apportionment. Atmospheric Environment, 40(15),
702 2690–2705. <https://doi.org/10.1016/j.atmosenv.2005.11.062>, 2006.

703 Irei, S., Takami, A., Hayashi, M., Sadanaga, Y., Hara, K., Kaneyasu, N., Sato K., Arakaki T.,
704 Hatakeyama S., Bandow H., Hikida T., and Shimono A.: Transboundary secondary organic
705 aerosol in western japan indicated by the $\delta^{13}\text{C}$ of water-soluble organic carbon and the m/z 44
706 signal in organic aerosol mass spectra. Environmental Science & Technology, 48(11), 6273-
707 6281, <https://doi.org/10.1021/es405362y>, 2014.

708 Jankowski, N., Schmidl, C., Marr, I. L., Bauer, H., and Puxbaum, H.: Comparison of methods for
709 the quantification of carbonate carbon in atmospheric PM10 aerosol samples. *Atmospheric*
710 *Environment*, 42(34), 8055–8064. <https://doi.org/10.1016/j.atmosenv.2008.06.012>, 2008.

711 Jimenez, J.L., Canagaratna, M.R., Donahue, N.M., Prevot, A.S.H., Zhang, Q., Kroll, J.H., DeCarlo,
712 P.F., Allan, J.D., Coe, H., Ng, N.L. and Aiken, A.C.: Evolution of Organic Aerosols in the
713 Atmosphere. *Science*, 326(5959), 1525–1529. <https://doi.org/10.1126/science.1180353>, 2009.

714 Kawamura, K., Kobayashi, M., Tsubonuma, N., Mochida, M., Watanabe, T., and Lee, M.: Organic
715 and inorganic compositions of marine aerosols from East Asia: Seasonal variations of water-
716 soluble dicarboxylic acids, major ions, total carbon and nitrogen, and stable C and N isotopic
717 composition. *Geochemical Society Special Publications*, 9(C), 243–265.
718 [https://doi.org/10.1016/S1873-9881\(04\)80019-1](https://doi.org/10.1016/S1873-9881(04)80019-1), 2004.

719 Kirillova, E.N., Andersson, A., Sheesley, R.J., Krus å M., Praveen, P.S., Budhavant, K., Safai, P.D.,
720 Rao, P.S.P. and Gustafsson, Ö.: ¹³C- And ¹⁴C-based study of sources and atmospheric
721 processing of water-soluble organic carbon (WSOC) in South Asian aerosols. *Journal of*
722 *Geophysical Research Atmospheres*, 118(2), 614–626. <https://doi.org/10.1002/jgrd.50130>,
723 2013.

724 Kirillova, E. N., Andersson, A., Tiwari, S., Kumar Srivastava, A., Singh Bisht, D., and Gustafsson,
725 Ö.: Water-soluble organic carbon aerosols during a full New Delhi winter: Isotope-base source
726 apportionment and optical properties. *Journal of Geophysical Research D: Atmospheres*, 119,
727 3476–3485. <https://doi.org/10.1002/2013JD021272>. Received, 2014.

728 Kirillova, E. N., Sheesley, R. J., Andersson, A., and Gustafsson, Ö. : Natural Abundance ¹³C and
729 ¹⁴C Analysis of Water-Soluble Organic Carbon in Atmospheric. *Analytical Chemistry*, 82(19),
730 7973–7978. <https://doi.org/10.1029/2006GL028325>, 2010.

731 Kong, S., Li, X., Li, L., Yin, Y., Chen, K., Yuan, L., Zhang, Y., Shan, Y. and Ji, Y.: Variation of
732 polycyclic aromatic hydrocarbons in atmospheric PM_{2.5} during winter haze period around
733 2014 Chinese Spring Festival at Nanjing: Insights of source changes, air mass direction and
734 firework particle injection. *Science of the Total Environment*, 520, 59–72.
735 <https://doi.org/10.1016/j.scitotenv.2015.03.001>, 2015.

736 Lang, S. Q., Bernasconi, S. M., and Früh-Green, G. L.: Stable isotope analysis of organic carbon in
737 small (µg C) samples and dissolved organic matter using a GasBench preparation device.
738 *Rapid Communications in Mass Spectrometry*, 26(1), 9–16. <https://doi.org/10.1002/rcm.5287>,
739 2012.

740 Liang, L.L., Guenter, E., Duan, F.K., Ma, Y.L., Cheng, Y., Du, Z.Y. and He, K.B.: Composition
741 and Source Apportionments of Saccharides in Atmospheric Particulate Matter in Beijing.
742 *Huanjing Kexue/Environmental Science* 36, no. 11: 3935–42.
743 <https://doi.org/10.13227/j.hjcx.2015.11.001>, 2015.

744 Martinelli, L. A., Camargo, P. B., Lara, L. B. L. S., Victoria, R. L., and Artaxo, P.: Stable carbon
745 and nitrogen isotopic composition of bulk aerosol particles in a C4 plant landscape of
746 southeast Brazil. *Atmospheric Environment*, 36(14), 2427–2432.
747 [https://doi.org/10.1016/S1352-2310\(01\)00454-X](https://doi.org/10.1016/S1352-2310(01)00454-X), 2002.

748 Martinez, R. E., Williams, B. J., Zhang, Y., Hagan, D., Walker, M., Kreisberg, N. M., Hering S. V.,
749 Hohaus T., Jayne J. T., Worsnop D. R.: Development of a volatility and polarity separator
750 (VAPS) for volatility- and polarity-resolved organic aerosol measurement. *Aerosol Science*
751 *and Technology*, 50(3), 255–271. <https://doi.org/10.1080/02786826.2016.1147645>, 2016.

752 Mills, N.L., Donaldson, K., Hadoke, P.W., Boon, N.A., MacNee, W., Cassee, F.R., Sandström, T.,
753 Blomberg, A. and Newby, D.E.: Adverse cardiovascular effects of air pollution. *Nature*
754 *Clinical Practice Cardiovascular Medicine*, 6(1), 36–44.
755 <https://doi.org/10.1038/ncpcardio1399>, 2009.

756 Miyazaki, Y., Fu, P. Q., Kawamura, K., Mizoguchi, Y., Yamanoi, K.: Seasonal variations of stable
757 carbon isotopic composition and biogenic tracer compounds of water-soluble organic aerosols
758 in a deciduous forest. *Atmospheric Chemistry and Physics*, 12:1367-1376, 10.1016/S0378-
759 4274(98)80829-1, 2012.

760 Miyazaki, Y., Kawamura, K., Jung, J., Furutani, H., and Uematsu, M.: Latitudinal distributions of
761 organic nitrogen and organic carbon in marine aerosols over the western North Pacific.
762 *Atmospheric Chemistry and Physics*, 11(7), 3037–3049. [https://doi.org/10.5194/acp-11-3037-](https://doi.org/10.5194/acp-11-3037-2011)
763 2011, 2011.

764 Myhre, G.: Consistency between satellite-derived and modeled estimates of the direct aerosol effect.
765 *Science*, 325(5937), 187–190. DOI: 10.1126/science.1174461, 2009.

766 Nina BrünicheOlsen, Ulstrup J . Quantum theory of kinetic isotope effects in proton transfer
767 reactions[J]. *Journal of the Chemical Society Faraday Transactions Physical Chemistry in*
768 *Condensed Phases*, 1979, 75(75):205-226.

769 Osada, K., Kido, M., Nishita, C., Matsunaga, K., Iwasaka, Y., & Nagatani, M., Nakada H.:
770 Temporal variation of water-soluble ions of free tropospheric aerosol particles over central
771 japan. *Tellus Series B-chemical & Physical Meteorology*, 59(4), 742–754,
772 <https://10.1111/j.1600-0889.2007.00296.x>, 2007.

773 Park, S. S., Schauer, J. J., and Cho, S. Y.: Sources and their contribution to two water-soluble
774 organic carbon fractions at a roadway site. *Atmospheric Environment*, 77, 348–357.
775 <https://doi.org/10.1016/j.atmosenv.2013.05.032>, 2013.

776 Pathak, R. K., Wang, T., Ho, K. F., and Lee, S. C.: Characteristics of summertime PM_{2.5} organic
777 and elemental carbon in four major Chinese cities: Implications of high acidity for water-
778 soluble organic carbon (WSOC). *Atmospheric Environment*, 45(2), 318–325.
779 <https://doi.org/10.1016/j.atmosenv.2010.10.021>, 2011.

780 Pavuluri, C. M., and Kawamura, K.: Evidence for ¹³C-enrichment in oxalic acid via iron
781 catalyzed photolysis in aqueous phase. *Geophysical Research Letters*, 39(3), 1–6.
782 <https://doi.org/10.1029/2011GL050398>, 2012.

783 Pavuluri C. M., Kawamura K.: Seasonal changes in TC and WSOC and their ¹³C isotope ratios in
784 Northeast Asian aerosols: land surface–biosphere–atmosphere interactions. *Acta Geochimica*,
785 36:355-358, <http://doi.org/10.1007/s11631-017-0157-3>, 2017.

786 Pavuluri, C. M., Kawamura, K., Swaminathan, T., and Tachibana, E.: Stable carbon isotopic
787 compositions of total carbon, dicarboxylic acids and glyoxylic acid in the tropical Indian
788 aerosols: Implications for sources and photochemical processing of organic aerosols. *Journal*
789 *of Geophysical Research Atmospheres*, 116(18), 1–10.
790 <https://doi.org/10.1029/2011JD015617>, 2011.

791 Polissar, P. J., Fulton, J. M., Junium, C. K., Turich, C. C., and Freeman, K. H.: Measurement of ¹³
792 C and ¹⁵ N Isotopic Composition on Nanomolar Quantities of C and N. *Analytical Chemistry*,
793 81(2), 755–763. <https://doi.org/10.3354/meps240085.water>, 2009.

794 Qin, X., Zhang, Z. F., Li, Y. W., Shen, Y., & Zhao, S. H... Sources analysis of heavy metal aerosol
795 particles in north suburb of nanjing. *Environmental Science*. 37(12): 4467-4474,
796 <http://10.13227/j.hjcx.201605237,2016>.

797 Ramanathan, V., Crutzen, P. J., Kiehl, J. T., and Rosenfeld, D.: Aerosols, climate, and the
798 hydrological cycle. *Science*, 294(5549), 2119–2124. DOI: 10.1126/science.1064034, 2001.

799 Rudolph, J.: *Gas Chromatography-Isotope Ratio Mass Spectrometry. Volatile Organic*
800 *Compounds in the Atmosphere*, 388–466. Blackwell Publishing: Oxford, UK, 2007.

801 Rudolph, J., Czuba, E., Norman, A. L., Huang, L., and Ernst, D.: Stable carbon isotope composition
802 of nonmethane hydrocarbons in emissions from transportation related sources and
803 atmospheric observations in an urban atmosphere. *Atmospheric Environment*, 36(7), 1173–
804 1181. [https://doi.org/10.1016/S1352-2310\(01\)00537-4](https://doi.org/10.1016/S1352-2310(01)00537-4), 2002.

805 Rudolph, J., Anderson R. S., Czapiewski K. V., Czuba E., Ernst D., Gillespie T., Huang L., Rigby
806 C., and Thompson A. E.: The stable carbon isotope ratio of biogenic emissions of isoprene
807 and the potential use of stable isotope ratio measurements to study photochemical processing
808 of isoprene in the atmosphere. *Journal of Atmospheric Chemistry*, 44(1), 39–55,
809 <http://10.1023/A:1022116304550>, 2003.

810 Saarikoski, S., Timonen, H., Saarnio, K., Aurela, M., Järvi, L., Keronen, P., Kerminen, V.M. and
811 Hillamo, R.: Sources of organic carbon in fine particulate matter in northern European urban
812 air. *Atmospheric Chemistry and Physics*, 8(20), 6281–6295. [https://doi.org/10.5194/acp-8-](https://doi.org/10.5194/acp-8-6281-2008)
813 [6281-2008](https://doi.org/10.5194/acp-8-6281-2008), 2008.

814 Sakugawa, H., Kaplan, I.R.: Stable carbon isotope measurements of atmospheric organic acids in
815 Los Angeles, California. *Geophysical Research Letters*, 22, 1509–1512,
816 <https://doi.org/10.1029/95GL01359,1995>

817 Sannigrahi, P., Sullivan, A. P., Weber, R. J., and Ingall, E. D.: Characterization of water-soluble
818 organic carbon in urban atmospheric aerosols using solid-state C-13 NMR spectroscopy,
819 *Environ. Sci. Technol.*, 40, 666-672, 2006

820 Sharp, J. H.: Total organic carbon in seawater - comparison of measurements using persulfate
821 oxidation and high temperature combustion. *Marine Chemistry*, 1(3), 211–229.
822 [https://doi.org/10.1016/0304-4203\(73\)90005-4](https://doi.org/10.1016/0304-4203(73)90005-4), 1973.

823 Smith, B. N., and Epstein, S.: Two Categories of ¹³C/¹²C Ratios for Higher Plants. *Plant*
824 *Physiology*, 47(3), 380–384. <https://doi.org/10.1104/pp.47.3.380>, 1971.

825 Sousa Moura, J. mauro, Martens, C. S., Moreira, M. Z., Lima, R. L., Sampaio, I. C. G., Mendlovitz,
826 H. P., and Menton, M. C.: Spatial and seasonal variations in the stable carbon isotopic
827 composition of methane in stream sediments of eastern Amazonia. *Tellus B: Chemical and*
828 *Physical Meteorology*, 60(1), 21–31. <https://doi.org/10.1111/j.1600-0889.2007.00322.x>, 2008.

829 Sullivan, A. P., Weber, R. J., Clements, A. L., Turner, J. R., Bae, M. S., and Schauer, J. J.: A method
830 for on-line measurement of water-soluble organic carbon in ambient aerosol particles: Results
831 from an urban site. *Geophysical Research Letters*, 31(13), 14–17.
832 <https://doi.org/10.1029/2004GL019681>, 2004.

833 Suto, N., Kawashima H.: Online wet oxidation/isotope ratio mass spectrometry method for
834 determination of stable carbon isotope ratios of water - soluble organic carbon in particulate

835 matter. *Rapid Communications in Mass Spectrometry*, 32(19): 1668-1674,
836 <http://doi.org/10.1002/rcm.8240>, 2018.

837 Ten Brink, H., Maenhaut, W., Hitenberger, R., Gnauk, T., Spindler, G., Even, A., Chi, X., Bauer,
838 H., Puxbaum, H., Putaud, J.P. and Tursic, J: INTERCOMP2000: The comparability of
839 methods in use in Europe for measuring the carbon content of aerosol. *Atmospheric*
840 *Environment*, 38(38), 6507–6519. <https://doi.org/10.1016/j.atmosenv.2004.08.027>, 2004.

841 Trolier, M. , White, J. W. C., Tans, P. P., Masarie, K. A., Gemery, P. A.: Monitoring the isotopic
842 composition of atmospheric CO₂: Measurements from the NOAA Global Air Sampling
843 Network. *Journal of Geophysical Research: Atmospheres*, 101(D20),
844 <https://doi.org/10.1029/96JD02363>, 1996.

845 Turekian, V. C., Macko, S., Ballentine, D., Swap, R. J., Garstang, M.: Causes of bulk carbon and
846 nitrogen isotopic fractionations in the products of vegetation burns: Laboratory studies.
847 *Chemical Geology*, 152(1-2):181-192. [http://doi.10.1016/S0009-2541\(98\)00105-3](http://doi.10.1016/S0009-2541(98)00105-3), 1998.

848 Wang, G., Xie, M., Hu, S., Gao, S., Tachibana, E., and Kawamura, K.: Dicarboxylic acids, metals
849 and isotopic compositions of C and N in atmospheric aerosols from inland China: Implications
850 for dust and coal burning emission and secondary aerosol formation. *Atmospheric Chemistry*
851 *and Physics*, 10(13), 6087–6096. <https://doi.org/10.5194/acp-10-6087-2010>, 2010.

852 Wang, H., Kawamura, K., and Shooter, D.: Wintertime organic aerosols in Christchurch and
853 Auckland, New Zealand: Contributions of residential wood and coal burning and petroleum
854 utilization. *Environmental Science and Technology*, 40(17), 5257–5262.
855 <https://doi.org/10.1021/es052523i>, 2006.

856 Wang, Y., Jia, C., Tao, J., Zhang, L., Liang, X., Ma J., Gao H., Huang T., Zhang K.: Chemical
857 characterization and source apportionment of pm_{2.5} in a semi-arid and petrochemical-
858 industrialized city, northwest china. *Science of The Total Environment*, 573, 1031-1040,
859 [10.1016/j.scitotenv.2016.08.179](https://doi.org/10.1016/j.scitotenv.2016.08.179), 2016.

860 Weber, R. J., Sullivan, A. P., Peltier, R. E., Russell, A., Yan, B., Zheng, M., de Gouw, J., Warneke,
861 C., Brock, C., Holloway, J. S., Atlas, E. L., and Edgerton, E.: A study of secondary organic
862 aerosol formation in the anthropogenic-influenced southeastern United States, *J. Geophys.*
863 *Res.*, 112, D13302, 2007.

864 Werner, R. A., Bruch, B. A., and Brand, W. A.: ConFlo III - an interface for high precision $\delta^{13}\text{C}$
865 and $\delta^{15}\text{N}$ analysis with an extended dynamic range. *Rapid Communications in Mass*
866 *Spectrometry*, 13(13), 1237–1241. [https://doi.org/10.1002/\(SICI\)1097-](https://doi.org/10.1002/(SICI)1097-0231(19990715)13:13<1237::AID-RCM633>3.0.CO;2-C)
867 [0231\(19990715\)13:13<1237::AID-RCM633>3.0.CO;2-C](https://doi.org/10.1002/(SICI)1097-0231(19990715)13:13<1237::AID-RCM633>3.0.CO;2-C), 1999.

868 Widory, D.: Combustibles, fuels and their combustion products: A view through carbon isotopes.
869 *Combustion Theory and Modelling*, 10(5), 831–841.
870 <https://doi.org/10.1080/13647830600720264>, 2006.

871 Wozniak, A. S., Bauer, J. E., Sleighter, R. L., Dickhut, R. M., and Hatcher, P. G.: Molecular
872 characterization of aerosol-derived water soluble organic carbon using ultrahigh resolution
873 electrospray ionization Fourier transform ion cyclotron resonance mass spectrometry.
874 *Atmospheric Chemistry and Physics*, 8(2), 5099–5111. [https://doi.org/10.5194/acp-8-5099-](https://doi.org/10.5194/acp-8-5099-2008)
875 [2008](https://doi.org/10.5194/acp-8-5099-2008), 2008.

876 Yu, S., Zhang, Q., Yan, R., Wang, S., Li, P., & Chen, B., Liu W., Zhang X.: Origin of air pollution
877 during a weekly heavy haze episode in hangzhou, china. *Environmental Chemistry Letters*,
878 12(4), 543-550, [10.1007/s10311-014-0483-1](https://doi.org/10.1007/s10311-014-0483-1), 2014.

879 Zeng, Y., & Hopke, P. K.: A study of the sources of acid precipitation in ontario, canada.
880 Atmospheric Environment, 23(7), 1499-1509, 10.1016/0004-6981(89)90409-5,1989.

881 Zhang, F., Cheng, H. R., Wang, Z. W., Lv, X. P., Zhu, Z. M., & Zhang, G., et al.: Fine particles (pm
882 2.5) at a cawnet background site in central china: chemical compositions, seasonal variations
883 and regional pollution events. Atmospheric Environment, 86(3), 193-202,
884 10.1016/j.atmosenv.2013.12.008, 2014.

885 Zhang, R., Jing, J., Tao, J., Hsu, S. C., Wang, G., & Cao, J. J., Lee C. S. L., Zhu L., Chen Z. M.,
886 Zhao Y., Shen Z. X.: Chemical characterization and source apportionment of pm2.5 in Beijing:
887 seasonal perspective. Atmospheric Chemistry and Physics, 13(14), 7053-7074, 10.5194/acp-
888 13-7053-2013, 2013.

889 Zhang, Y.L., El-Haddad, I., Huang, R.J., Ho, K.F., Cao, J.J., Han, Y.M., Zotter, P., Bozzetti, C.,
890 Daellenbach, K.R., Slowik, J.G., Salazar, G., Prévôt, A.S. and Szidat, S.: Large contribution
891 of fossil fuel derived secondary organic carbon to water soluble organic aerosols in winter
892 haze in China. Atmospheric chemistry and physics, 18(6), pp.4005-4017.
893 <https://doi.org/10.5194/acp-18-4005-2018>, 2018.

894 Zhang, Y.L., Li, J., Zhang, G., Zotter, P., Huang, R.J., Tang, J.H., Wacker, L., Prévôt, A.S. and
895 Szidat, S.: Radiocarbon-based source apportionment of carbonaceous aerosols at a regional
896 background site on Hainan Island, South China. Environmental Science and Technology,
897 48(5), 2651–2659. <https://doi.org/10.1021/es4050852>, 2014.

898 Zhou, Y., Guo, H., Lu, H., Mao, R., Zheng, H., and Wang, J.: Analytical methods and application
899 of stable isotopes in dissolved organic carbon and inorganic carbon in groundwater. Rapid
900 Communications in Mass Spectrometry, 29(19), 1827–1835.
901 <https://doi.org/10.1002/rcm.7280>, 2015.

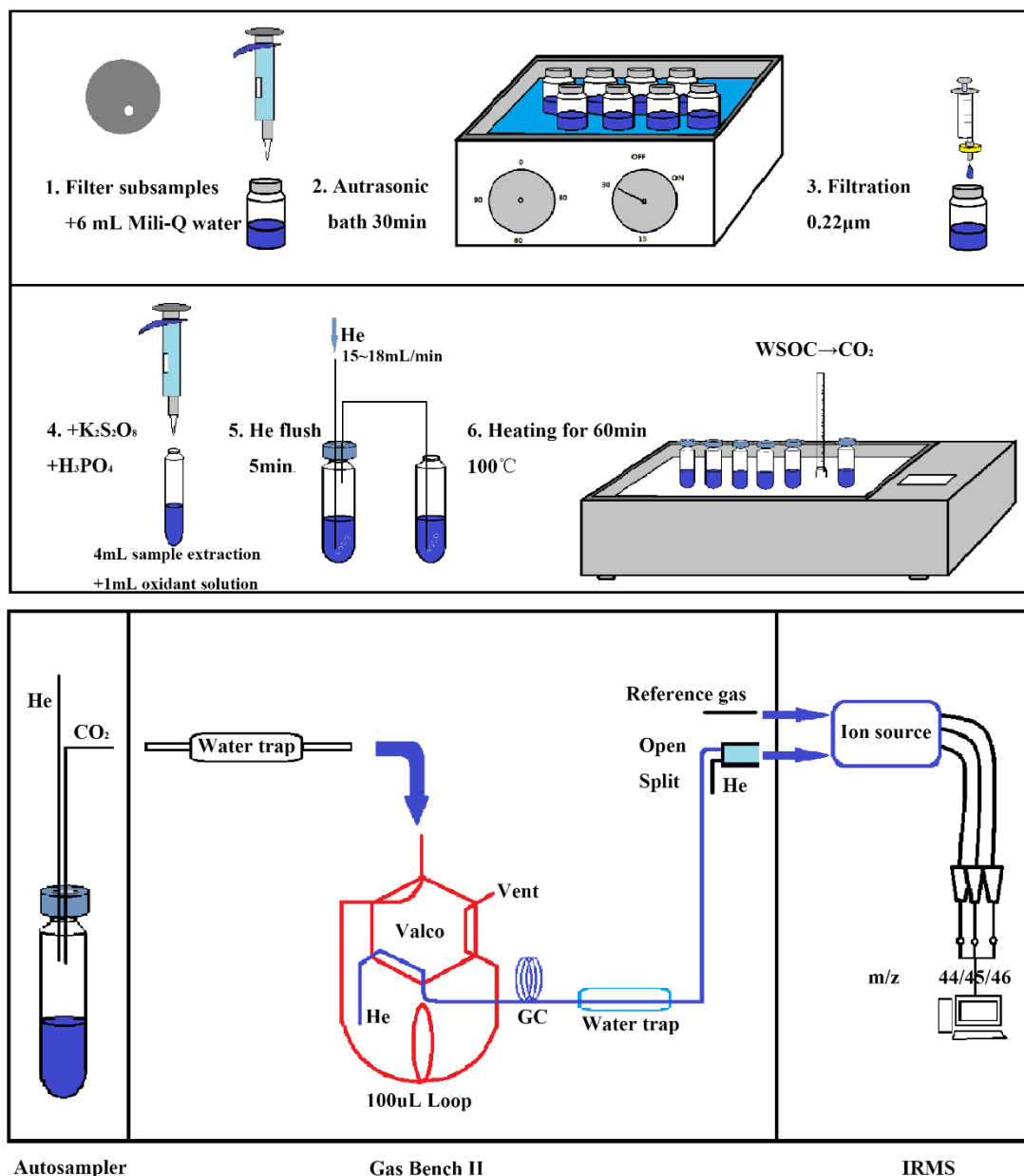
902

903 **Table 1.** Various blank preparation with results.

Identifier	Oxidant ^a	Acid ^b	C content (µgC)	δ ¹³ C(‰)
Mili-Q water	-	-	ND*	-
Mili-Q water	-	-	ND*	-
Mili-Q water +Acid-1	-	100 uL 85 % H ₃ PO ₄ , AR	0.04	-1.6
Mili-Q water +Acid-1	-	100 uL 85 % H ₃ PO ₄ , AR	0.04	-4.3
Mili-Q water +Acid-2	-	100 uL 85 % H ₃ PO ₄ , HPLC	0.03	-4.9
Mili-Q water +OX+Acid- 1	2.0 g K ₂ S ₂ O ₈	100 uL 85 % H ₃ PO ₄ , AR	0.63	-25.90
Mili-Q water +OX+Acid- 1	2.0 g K ₂ S ₂ O ₈	100 uL 85 % H ₃ PO ₄ , AR	0.54	-25.69
Mili-Q water +OX+Acid- 1	2.0 g K ₂ S ₂ O ₈	100 uL 85 % H ₃ PO ₄ , AR	0.46	-24.77
Mili-Q water +OX+Acid- 2	2.0 g K ₂ S ₂ O ₈	100 uL 85 % H ₃ PO ₄ , HPLC	0.63	-26.66
Mili-Q water +OX+Acid- 2	2.0 g K ₂ S ₂ O ₈	100 uL 85 % H ₃ PO ₄ , HPLC	0.56	-27.38
Mili-Q water +OX+Acid- 2	2.0 g K ₂ S ₂ O ₈	100 uL 85 % H ₃ PO ₄ , HPLC	0.58	-26.91

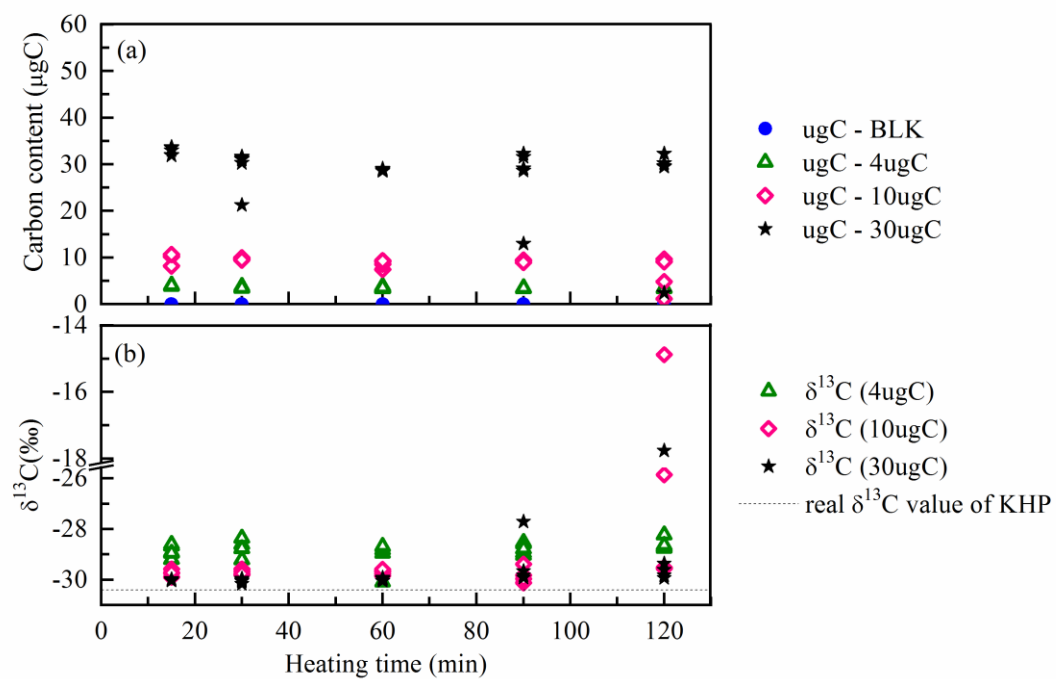
904 ^{a, b} oxidant and acid are added to 50 mL Mili-Q water.

905 ND* : Not detected



906

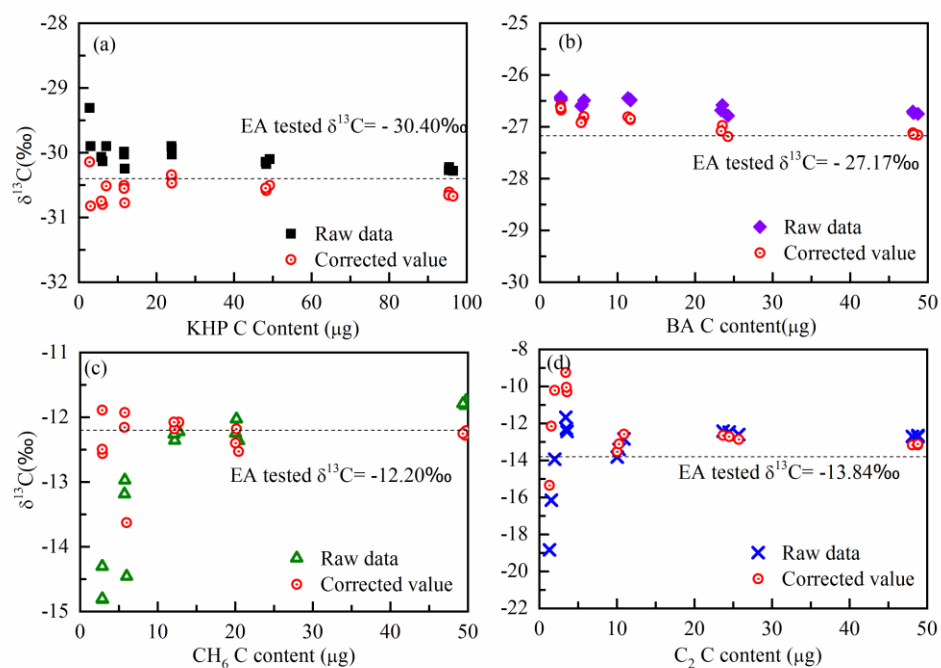
907 **Figure 1.** Schematic of the optimized method for the measurement of WSOC mass concentrations
 908 and the $\delta^{13}\text{C}_{\text{-wsoc}}$ values. (A filter disc is dissolved with 6mL Mili-Q water in a 20 mL pre-
 909 combusted glass bottle in the first step. After 30 minutes autrasonic bath, the WSOC extract is
 910 filtered with 0.22 µm syringe filter and transferred to another 20 mL pre-combusted glass bottle in
 911 step 3. 4 mL filtrate is transferred to a 12 mL pre-combusted glass vial which contains 1 mL oxidant
 912 solution (2.0g K₂S₂O₈ and 100 µL 85% H₃PO₄ dissolved in 50 mL Mili-Q water) in the vial in step
 913 4. Next, the mixed solution of WSOC extract and the oxidant solution is flushed with Helium at a
 914 flow rate of 15-18 mL min⁻¹ as shown in step 5. At last, the vials are heated for 60 minutes under
 915 100 °C in the sand bath pot (step 6.)



916

917 **Figure 2.** Carbon contents (a) and isotopic ratios (b) of KHP after different heating time.

918



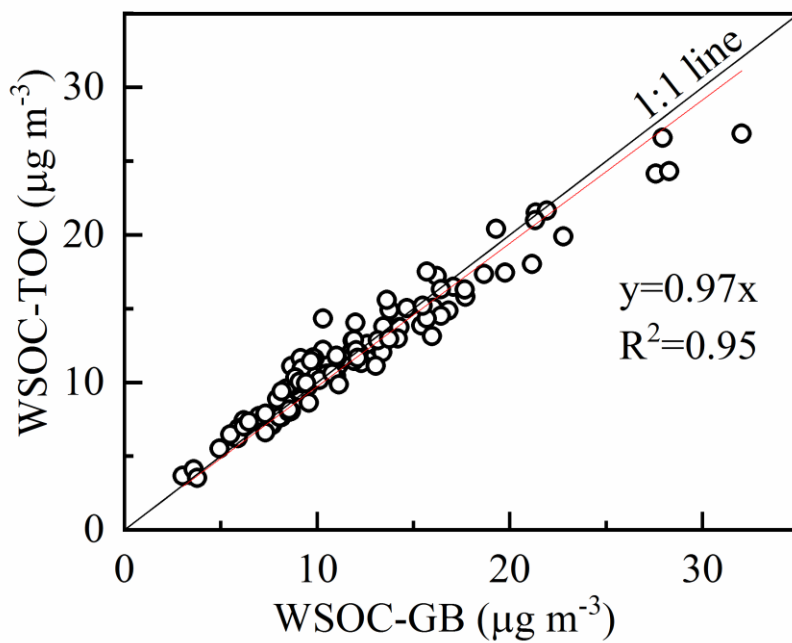
919

920 **Figure 3.** Isotope results before and after the two-step correction of the four standards.

921 (a. KHP, b. BA, c. CH_6 , d. C_2 . Red circle with a spot represents the two-step corrected isotopic

922 ratios; ■, ◆, ▲, × represent the raw data from Gas Bench II; the dotted line represents the blank

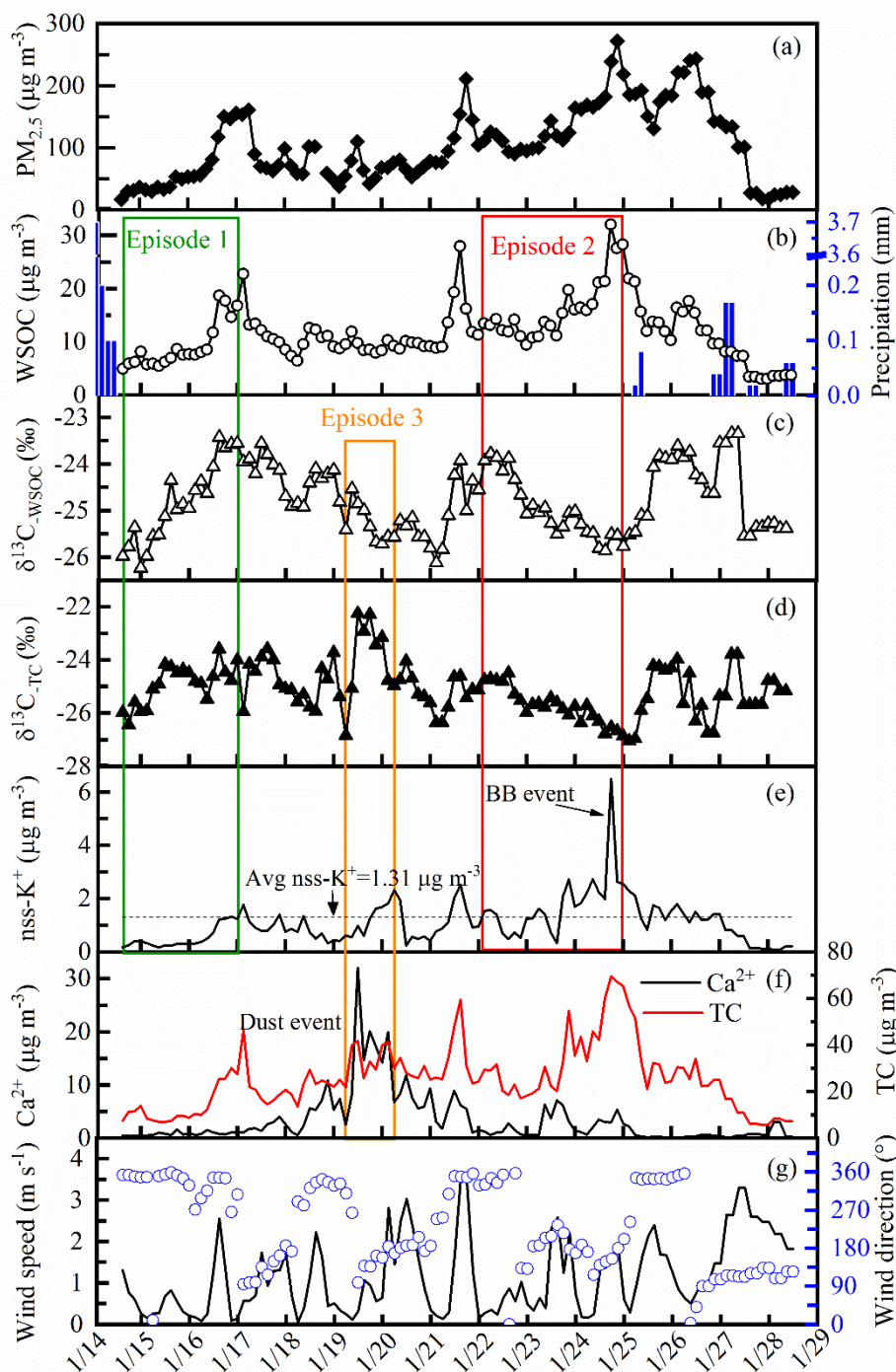
923 corrected $\delta^{13}\text{C}$ values tested by EA)



924

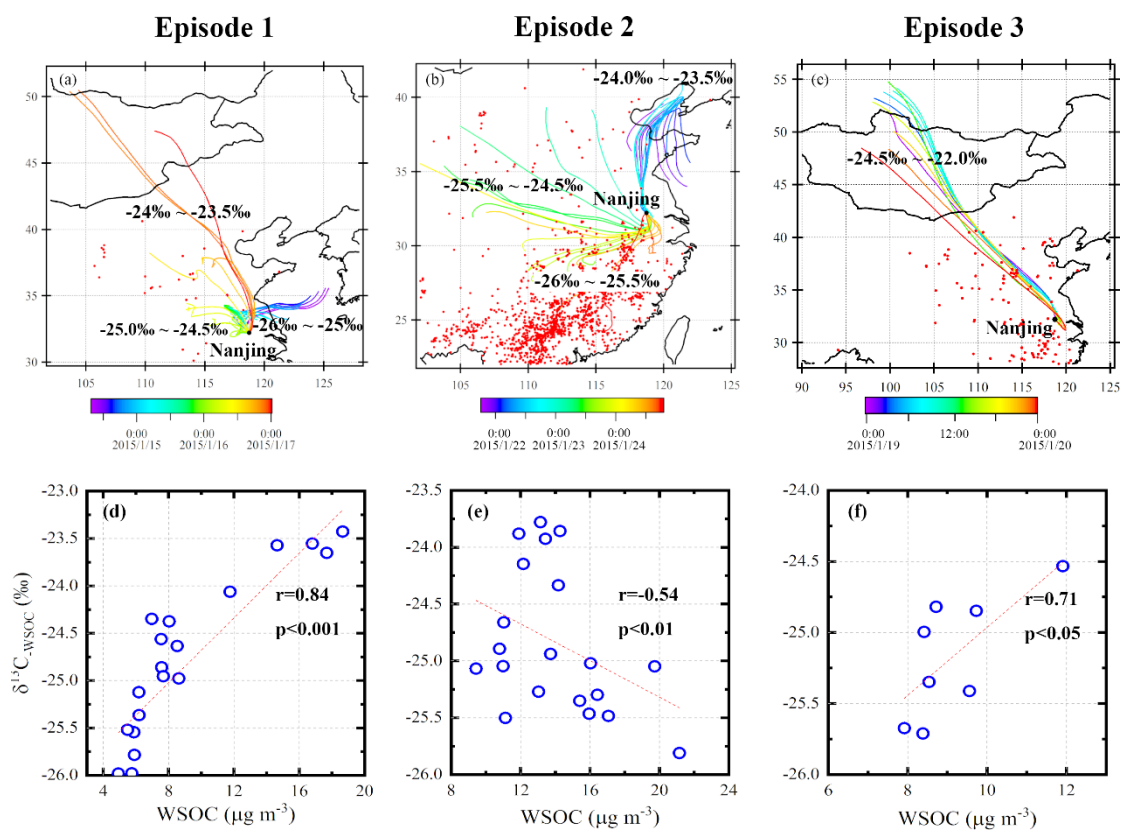
925 **Figure 4.** Correlation of WSOC mass concentrations measured with Gas Bench II - IRMS and
926 TOC analyzer.

927



928

929 **Figure 5.** Time series of PM_{2.5}, WSOC, precipitation, $\delta^{13}\text{C}$ values, nss-K⁺, Ca²⁺, TC, wind speed
 930 and wind direction at the sampling site during the studied period. (The time period framed with the
 931 rectangles is defined as the Episode 1 (green), the Episode 2 (red) and the Episode 3 (orange). The
 932 dotted line in 5e is the average value of nss-K⁺ during the studied period. The high concentration
 933 and intense increase of nss-K⁺ in the Episode 2 indicate a significant biomass burning (BB) event,
 934 and is marked with “BB event” in 5e. The similar trends of Ca²⁺ and TC suggest a dust event in the
 935 Episode 3.)



936

937 **Figure 6.** 48h-air mass back trajectories at 500m and MODIS fire maps in the three episodes and
 938 the corresponding relationship between WSOC and $\delta^{13}\text{C}_{\text{WSOC}}$.

939 (a, b and c represent the back trajectories and the fire maps of the Episode 1, 2 and 3, separately.

940 The colors of the back trajectories are marked according to the time of the specific trajectory. Red

941 points represent the fire spots in each episode obtained from the Fire Information for Resource

942 Management System (FIRMS) derived from the Moderate Resolution Imaging Spectroradiometer.

943 The ranges of the $\delta^{13}\text{C}$ values of the back trajectories are labeled: the marked isotopic ratios are the

944 $\delta^{13}\text{C}_{\text{WSOC}}$ values (for a and b) and the $\delta^{13}\text{C}_{\text{TC}}$ values (for c). d, e and f are the correlation between

945 WSOC and $\delta^{13}\text{C}_{\text{WSOC}}$ in each episode.)

946